Journal of Volcanology and Geothermal Research 324 (2016) 88–104

Contents lists available at ScienceDirect

Journal of Volcanology and Geothermal Research

journal homepage: www.elsevier.com/locate/jvolgeores

Physical, chemical and mineralogical evolution of the Tolhuaca geothermal system, southern Andes, Chile: Insights into the interplay between hydrothermal alteration and brittle deformation

Pablo Sanchez-Alfaro [a,b,*], Martin Reich [a,b], Gloria Arancibia [b,c], Pamela Pérez-Flores [b,c], José Cembrano [b,c], Thomas Driesner [d], Martin Lizama [a,b], Julie Rowland [e], Diego Morata [a,b], Christoph A. Heinrich [d], Daniele Tardani [a,b], Eduardo Campos [f]

[a] Department of Geology, Universidad de Chile, 8370450 Santiago, Chile
[b] Andean Geothermal Center of Excellence (CEGA), Universidad de Chile, Santiago, Chile
[c] Department of Structural and Geotechnical Engineering, Pontificia Universidad Católica de Chile, 7820436 Santiago, Chile
[d] Department of Earth Sciences, Swiss Federal Institute of Technology, ETH Zentrum NO, 8092 Zürich, Switzerland
[e] School of Environment, The University of Auckland, Auckland, New Zealand
[f] Departamento de Ciencias Geológicas, Universidad Católica del Norte, Antofagasta, Chile

ARTICLE INFO

Article history:
Received 29 January 2016
Received in revised form 16 May 2016
Accepted 18 May 2016
Available online 25 May 2016

Keywords:
Tolhuaca geothermal system
Fault-fracture networks
Hydrothermal alteration
Fluid inclusions
Liquiñe-Ofqui Fault System

ABSTRACT

In this study, we unravel the physical, chemical and mineralogical evolution of the active Tolhuaca geothermal system in the Andes of southern Chile. We used temperature measurements in the deep wells and geochemical analyses of borehole fluid samples to constrain present-day fluid conditions. In addition, we reconstructed the paleo-fluid temperatures and chemistry from microthermometry and LA-ICP-MS analysis of fluid inclusions taken from well-constrained parageneses in vein samples retrieved from a ~ 1000 m borehole core. Based on core logging, mineralogical observations and fluid inclusions data we identify four stages (S1–S4) of progressive hydrothermal alteration. An early heating event (S1) was followed by the formation of a clay-rich cap in the upper zone (<670 m) and the development of a propylitic alteration assemblage at greater depth (S2). Boiling, flashing and brecciation occurred later (S3), followed by a final phase of fluid mixing and boiling (S4). The evolution of hydrothermal alteration at Tolhuaca has produced a mineralogical, hydrological and structural vertical segmentation of the system through the development of a low-permeability, low-cohesion clay-rich cap at shallow depth. The quantitative chemical analyses of fluid inclusions and borehole fluids reveal a significant change in chemical conditions during the evolution of Tolhuaca. Whereas borehole (present-day) fluids are rich in Au, B and As, but Cu-poor (B/Na ~ $10^{0.5}$, As/Na ~ $10^{-1.1}$, Cu/Na ~ $10^{-4.2}$), the paleofluids trapped in fluid inclusions are Cu-rich but poor in B and As (B/Na ~ 10^{-1}, As/Na ~ $10^{-2.5}$, Cu/Na ~ $10^{-2.5}$ in average). We interpret the fluctuations in fluid chemistry at Tolhuaca as the result of transient supply of metal-rich, magmatically derived fluids where As, Au and Cu are geochemically decoupled. Since these fluctuating physical and chemical conditions at the reservoir produced a mineralogical vertical segmentation of the system that affects the mechanical and hydrological properties of host rock, we explored the effect of the development of a low-cohesion low-permeability clay cap on the conditions of fault rupture and on the long-term thermal structure of the system. These analyses were performed by using rock failure condition calculations and numerical simulations of heat and fluid flows. Calculations of the critical fluid pressures required to produce brittle rupture indicate that within the clay-rich cap, the creation or reactivation of highly permeable extensional fractures is inhibited. In contrast, in the deep upflow zone the less pervasive formation of clay mineral assemblages has allowed retention of rock strength and dilatant behavior during slip, sustaining high permeability conditions. Numerical simulations of heat and fluid flows support our observations and suggest that the presence of a low permeability clay cap has helped increase the duration of high-enthalpy conditions by a factor of three in the deep upflow zone at Tolhuaca geothermal system, when compared with an evolutionary scenario where a clay cap was not developed. Furthermore, our data demonstrate that the dynamic interplay between fluid flow, crack-seal processes and hydrothermal alteration are key factors in the evolution of the hydrothermal system, leading to the development of a high enthalpy reservoir at the flank of the dormant Tolhuaca volcano.

© 2016 Elsevier B.V. All rights reserved.

* Corresponding author at: Department of Geology, Universidad de Chile, 8370450 Santiago, Chile.
E-mail address: vsanchez@ing.uchile.cl (P. Sanchez-Alfaro).

http://dx.doi.org/10.1016/j.jvolgeores.2016.05.009
0377-0273/© 2016 Elsevier B.V. All rights reserved.

1. Introduction

The Andean volcanic arc of Chile represents one of the largest undeveloped geothermal provinces of the world, with an estimated potential of ~16,000 MW for at least 50 years (Aravena et al., 2016; Lahsen et al., 2015). Geothermal systems have been largely understudied in the Andes, and in particular, there is limited scientific information on the origin and evolution of active hydrothermal systems (Alam and Parada, 2013; Sanchez-Alfaro et al., 2015). A better understanding of the mineralogical, chemical and structural evolution of Andean geothermal systems is key to developing efficient and environmentally friendly exploration of energy resources with a regional focus (Moore and Simmons, 2013; Sanchez-Alfaro et al., 2015).

Because changes in the thermodynamic conditions of hydrothermal systems strongly affect mineral stability, it is possible to track the long-term temperature, pressure and fluid chemistry evolution of the system by analyzing mineral paragenesis (e.g., Browne, 1978). Mineralogical studies may reveal the main processes occurring during the development of geothermal reservoirs, such as heating, cooling and fluid mixing, among others (Browne, 1978; Moore et al., 2008; Simmons and Browne, 2000). The active precipitation of hydrothermal minerals often produces crack sealing and loss of permeability that inhibits efficient fluid flow (Davatzes and Hickman, 2010). An opposing effect is fault-fracture networks activity that episodically produces an enhancement of permeability in brittle rocks (Barton et al., 1998; Davatzes and Hickman, 2010; Hickman et al., 1997; Hanano, 2004; Meller and Kohl, 2014). In particular, it has been shown that the reactivation of optimally oriented and critically stressed fractures is an important mechanism in maintaining high reservoir permeability in some geothermal systems by opening new and preexistent fractures (Davatzes and Hickman, 2010; Hanano, 2004; Meller and Kohl, 2014). However, rocks with ductile behavior, such as hydrothermal clays, which are characterized by low permeability, commonly reduce the strength and the cohesion of the fractures (Dobson et al., 2003; Neuzil, 1994; Wyering et al., 2014). These conditions promote shear and inhibit dilatation of preexistent fractures, and therefore it has been suggested that in rocks that are pervasively altered to clays, deformation is not an efficient mechanism to enhance permeability (Davatzes and Hickman, 2010; Dobson et al., 2003; Meller and Kohl, 2014).

On a geothermal reservoir scale, the aforementioned processes lead to areas where brittle (e.g., quartz/calcite-filled) fracture networks correlate with enhanced fluid flow, while clay-bearing fault/fracture zones act as persistent barriers (Davatzes and Hickman, 2010; Meller and Kohl, 2014; Rowland and Sibson, 2004). Therefore, hydrothermal alteration and fault system activity compartmentalize geothermal systems and may both enhance or inhibit hydrothermal fluid flow (Davatzes and Hickman, 2010; Meller and Kohl, 2014; Nemčok et al., 2007; Rowland and Simmons, 2012). Although both permeability and mineralization are strongly affected by processes associated with heat-fluid–rock interaction, a model that integrates the feedback mechanisms involved and their effect on conditions for fault rupture is currently lacking for geothermal reservoirs in the Andes. Furthermore, the effect on the duration and thermal structure of the hydrothermal system that such interaction may produce – and thus, the sustainability of the geothermal energy resource in the Andes – remains largely unconstrained. The goal of this study is therefore to establish the physical, chemical and mineralogical evolution of an active Andean geothermal system and to explore the effects of the interplay between heat–fluid–rock interaction and brittle deformation in the evolution of high enthalpy systems in this seismically active region.

An excellent natural laboratory to study the evolution of Andean hydrothermal systems is the Andean Cordillera of central-southern Chile, where the abundant geothermal resources have been recently explored, and thus subsurface mineralogical, geochemical and geophysical data is accessible (Aravena et al., 2016; Lahsen et al., 2010). This region also offers an opportunity to explore feedbacks between brittle deformation and heat-fluid–rock interaction because active hydrothermal systems occur in close spatial relationship with active volcanism as well as major seismically active fault systems (Cembrano and Lara, 2009). In the southern Andes Volcanic Zone, between 39° and 46°S, the volcanic and hydrothermal activity is controlled by the NNE-trending, 1200 km long Liquiñe-Ofqui Fault System (LOFS) and the NW-striking Andean Transverse Faults (ATF), which host ~25% of geothermal features in the Chilean Andes (Lahsen et al., 2010; Sánchez et al., 2013; Sanchez-Alfaro et al., 2015). Within this setting, the active Tolhuaca geothermal field in the northern termination of the LOFS (Fig. 1) has recorded the typical sequence of hydrothermal alteration of high enthalpy systems (Melosh et al., 2012). Furthermore, the Tolhuaca geothermal system is one of the very few systems that have been drilled by geothermal companies in the whole region, with an estimated power potential of 70 MWe (Aravena et al., 2016). The deep exploration drilling performed by MRP Geothermal Chile Ltda (formerly GGE Chile SpA) allows the investigation of a hydrothermal system not yet affected by geothermal production or re-injection (Melosh et al., 2012; Melosh et al., 2010).

In this study, we unravel the physical, chemical and mineralogical evolution of the active Tolhuaca geothermal system. To achieve this goal, we first determined mineral paragenesis at Tolhuaca by using optical petrography and scanning electron microscopy (SEM) in veins and rock samples obtained from a deep (~1000 km) borehole core. In addition, temperature measurements in the deep wells and analyses of fluid samples retrieved from the reservoir were used to constrain present-day fluid conditions. We complemented this information by reconstructing the paleo-fluid temperature and chemistry from fluid inclusions microthermometry and LA-ICP-MS analyses of single fluid inclusions in representative assemblages.

In order to explore the effect of hydrothermal alteration on the mechanical behavior of altered rocks at Tolhuaca, we calculated the failure conditions for two end-member scenarios, an intact rock case and a low-cohesion, low-permeability clay-rich rock scenario. Since our calculations suggest that hydrothermal alteration may substantially inhibit secondary permeability creation we explore its consequences on the thermal structure of the Tolhuaca geothermal system. In particular, we modeled the impact of a low permeability clay cap on the evolution of pressure and temperature conditions in the reservoir by using numerical simulations of heat and fluid flow. By integrating these data, our analysis constrains the conditions leading to the development of high enthalpy geothermal resources in the Southern Andes.

2. Geological background

2.1. Tectono-magmatic setting

The main tectonic features in the southern Andes volcanic zone are the LOFS and the ATF (Fig. 1) (Lavenu and Cembrano, 1999; Rosenau et al., 2006; Perez-Flores et al., 2016). The LOFS is a major intra-arc fault system that dominates the SVZ between 38°S and 47°S (Cembrano, 1996; Rosenau et al., 2006; Perez-Flores et al., 2016). The LOFS accommodates strain along the intra-arc by dextral strike shearing along the NNE-striking master fault and normal and dextral strike–slip in subsidiary ENE-striking faults (Lavenu and Cembrano, 1999; Rosenau et al., 2006; Perez-Flores et al., 2016). Fault–slip data and stress tensors for Pleistocene deformation along the northern portion of the LOFS consistently show a subhorizontal maximum principal compressive stress (σ_{Hmax}) trending N60°E (Lavenu and Cembrano, 1999; Rosenau et al., 2006; Perez-Flores et al., 2016). NNE-striking master faults are favorably orientated for dextral shear with respect to the prevailing stress field and ENE-striking tension fractures likely form under relatively low differential stress (Cembrano and Lara, 2009; Lavenu and Cembrano, 1999; Perez-Flores et al., 2016). In the above-described tectonic setting, the WNW-striking faults of the ATF are severely misorientated for shear with respect to the prevailing stress field and have been interpreted as crustal weaknesses associated with pre-

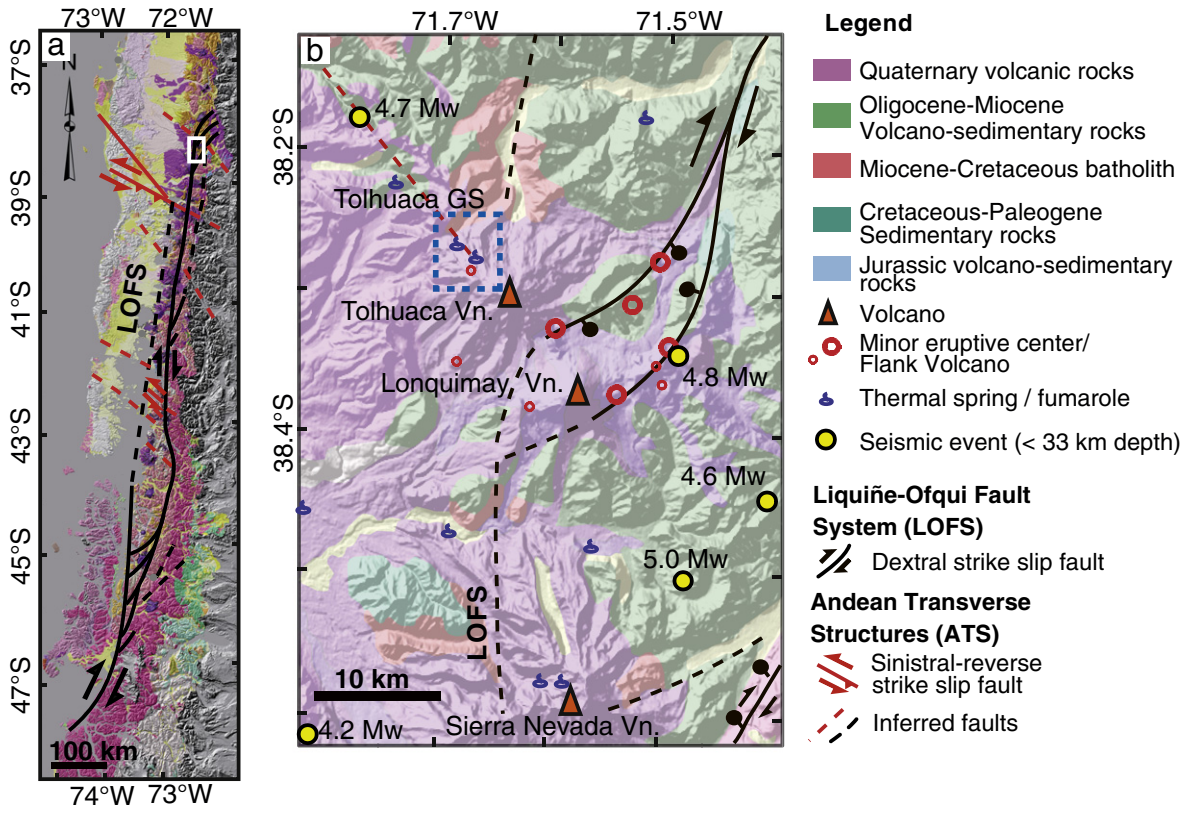

Fig 1. Geodynamic and structural setting of the Tolhuaca geothermal system. a, Digital Elevation Model showing the location and extent of the Liquiñe-Ofqui Fault System (LOFS; in black) and the NW-trending Andean Transverse Faults (ATF; in red) (Sánchez et al., 2013). b, Simplified geological map and major structural systems LOFS and ATF (Perez-Flores et al., 2013).

Andean faults reactivated as sinistral-reverse strike–slip faults during arc development (Cembrano and Lara, 2009; Rosenau et al., 2006; Perez-Flores et al., 2016). In this context, the nature and origin of hydrothermal systems is strongly dependent on structurally controlled heat transfer mechanisms that define contrasting magmatic-tectonic-hydrothermal domains (Sánchez et al., 2013). In particular, the Tolhuaca volcano is likely to be related to the ATF which provides the suitable conditions for the development of magma reservoirs and magma differentiation (Cembrano and Lara, 2009). In the area near the Tolhuaca volcano, the basement of the Pleistocene–Holocene volcanic arc is Miocene volcano-sedimentary rocks (Fig. 1), which have high intrinsic porosity and permeability and thus enhance the development of a hydrothermal reservoirs (Cembrano and Lara, 2009). Plutonic rocks associated with the Miocene batholith are relatively impermeable unless highly fractured.

The Tolhuaca volcano is a glacially scoured composite stratovolcano of late-Pleistocene to Holocene age that rises ~900 m over the basement (Lohmar et al., 2012; Thiele et al., 1987). In the summit there are several NW-trending aligned craters with different degrees of preservation that indicate a migration of the volcanic activity from SE towards the NW (Thiele et al., 1987). The latest eruptive phases are at the NW extreme and correspond to a NW-trending fissure (~2 km long) and a pyroclastic cone. Lavas are predominantly basaltic andesites and andesites, with minor presence of basalts and dacites (Thiele et al., 1987).

2.2. The Tolhuaca geothermal system

The Tolhuaca geothermal system is located on the northwest flank of the Tolhuaca volcano and is characterized by several surficial thermal manifestations including solfatara areas with fumaroles, boiling pools and hot springs (Fig. 1). Geothermal exploration campaigns comprising surface mapping, fluid geochemistry analyses, resistivity (MT) measurements and borehole logging have revealed the existence of a high enthalpy reservoir in the system (Melosh et al., 2012; Melosh et al., 2010). Two slim holes (Tol-1 and Tol-2) and two larger diameter wells (Tol-3 and Tol-4) were drilled down to 2117 m vertical depth. Of the two slim holes, rock cores were retrieved during drilling only from Tol-1; it is important to emphasize that this is the only available diamond drilled core material at Tolhuaca that can be used to undertake a detailed mineralogical analysis of veins and fractures (in wells Tol-2, Tol-3 and Tol-4 only drill cutting samples were retrieved). Temperature logging and fluid samples suggest the presence of a geothermal reservoir at c.a. 1.5 km depth, at liquid-saturated conditions with temperatures up to 300 °C and a strong meteoric water component (Melosh et al., 2012). The main reservoir is overlain by a steam heated aquifer at shallow depths that reaches up to 160 °C and controls the nature of most of the hot springs (Melosh et al., 2012; Melosh et al., 2010).

Rocks at Tolhuaca boreholes are mainly of basaltic andesite composition, although the whole rock chemical range varies from basalt to dacites (Lohmar et al., 2012). Deposit types observed are mainly lavas and related breccias, volcaniclastics and minor tuffs (Fig. 2). Hyaloclastites and pillow breccia occur at different levels in the Tol-1 core, indicating that lavas erupted during several time periods were in contact with glacial ice and/or water (Lohmar et al., 2012). Lohmar et al. (2012) suggest that the thick sequence dominated by volcaniclastic rocks in most of the bottom portions of the deepest wells (Tol-3 and Tol-4) may correspond to the Miocene Cura Mallín Formation (Niemeyer and Muñoz, 1983). In Tol-3 well, the Malleco and Cura Mallín formations are cut by numerous weakly altered, fine- to medium-grained intrusions that are interpreted as feeders to the Tolhuaca volcanics (Lohmar et al., 2012).

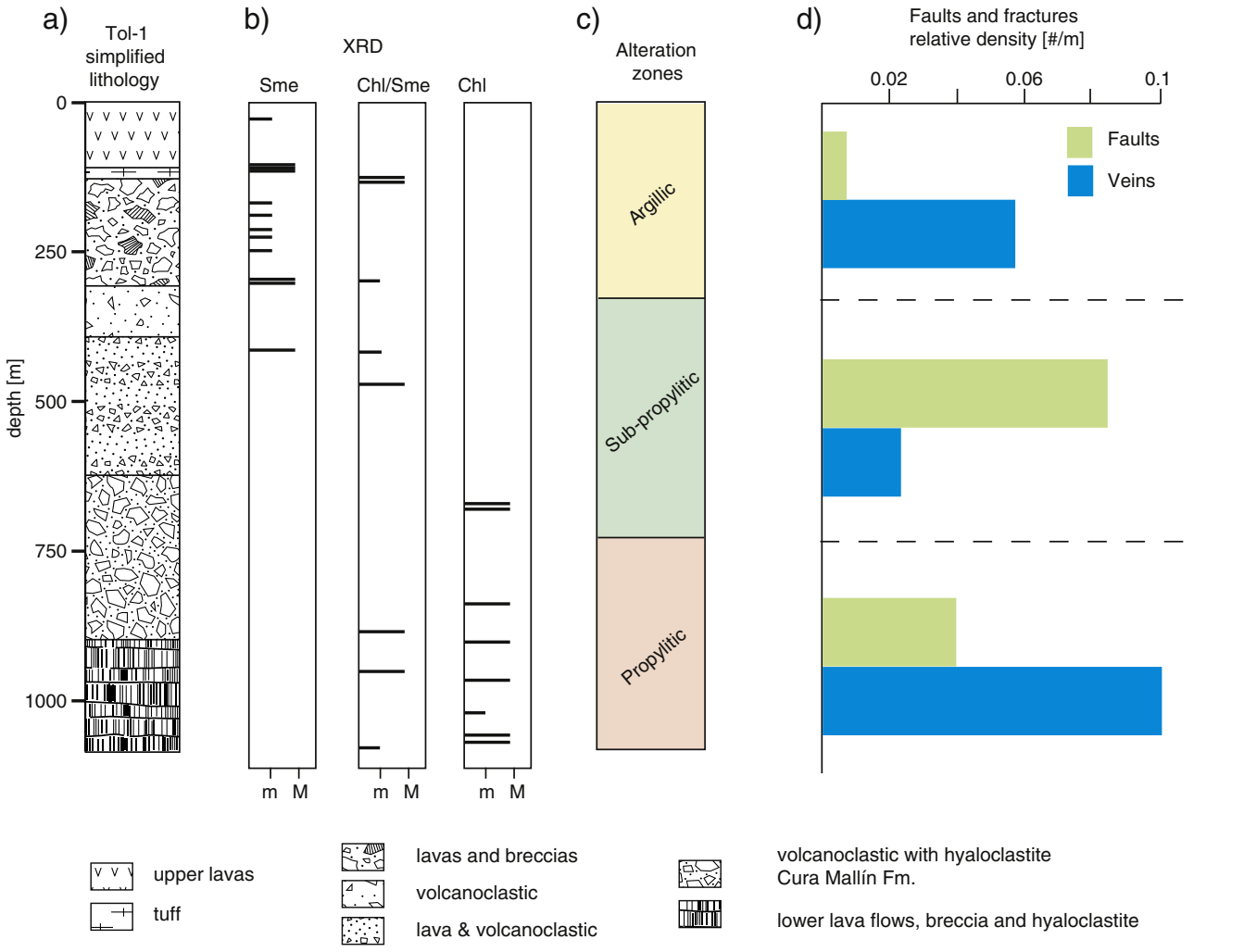

Fig. 2. Main features of the Tol-1 well. a) Simplified lithology. b) X-ray diffraction (XRD) data from Melosh et al. (2010, 2012). Relative abundances of selected phyllosilicate minerals are shown as minor (m) and major (M) concentrations. Sme: Smectite, Chlorite: Chl c) Hydrothermal alteration zones defined by Sanchez et al. (2013). d) Average of fault and fracture density for the three hydrothermal alteration zones (modified from Sanchez et al., 2013).

Surface hydrothermal alteration shows widespread acid-sulfate style mineralization towards the summit of Tolhuaca Volcano. Argillic alteration is scattered at the surface in the main part of the geothermal prospect (Melosh et al., 2010). Based on thin section and XRD analyses of the Tol-1 core (Fig. 2), Melosh et al. (2012) defined an upper zone of argillic alteration (20 to 450 m), an intermediate zone with phyllic alteration (450 to 650 m), and a deeper zone of propylitic alteration (≥650 m). These authors characterized argillic alteration facies by Fe-oxides + chlorite + calcite + clay ± quartz ± pyrite, whereas high temperature propylitic facies are composed of chlorite + epidote + calcite ± pyrite ± quartz ± zeolites mineral assemblages.

A detailed structural logging of the Tol-1 core was performed to identify mesoscopic faults, veins and fractures. The Tol-1 core was not oriented when recovered and therefore, core reorientation by paleomagnetic methods was performed to establish the geometry and kinematics of the fracture network at Tolhuaca (Perez-Flores et al., 2013). Paleomagnetic reorientation of core segments was obtained after calculating a stable remnant magnetization vector by using thermal (up to 700 °C) and alternating field demagnetization (up to 90mT on steps of 2mT) methods. Structural mapping of the reoriented core shows N50°–60°E-striking preferential vein orientation. In addition, N40°–50°E and N60°–70°W-striking preferential fault orientations were identified. Kinematic analysis of fault-slip data shows a N60°E-striking bulk fault plane solution with normal strain regime (Perez-Flores et al., 2013; Perez-Flores et al., *in prep*). The vein and fault orientations show strain axes that are in agreement with the regional stress field (σ_{max} N238°E; Lavenu and Cembrano, 1999; Rosenau et al., 2006; Perez-Flores et al., 2016).

Detailed logging of the Tol-1 drill core reveals the occurrence of three structural zones with contrasting features in veins, veins and fractures: (1) a shallow level (0–300 m) characterized by a relatively high frequency of open fractures, normal faults and veins and absence of shear fractures. At the base of this zone (~301 m), a 30 cm-thick cataclastic zone underlies 10 m of abundant hydrothermal breccias (Perez et al., 2012; Sanchez et al., 2013). (2) An intermediate level (300–670 m) characterized by the highest shear fracture frequency, and few quartz and calcite veins. Most of the low-angle (≤35°) structures measured during core logging are restricted to this intermediate level. (3) The deepest level (>670 m) presents a low-shear fracture density and the highest vein frequency (Fig. 2). The aforementioned veins are filled by quartz, calcite and epidote.

Borehole temperature and temperature gradient data from the deep wells reveal that hydrology and heat transfer regime is vertically segmented (Fig. 3). The shallow level (0–300 m) presents a steep temperature gradient (locally up to 150 °C/km) and hosts a steam-heated

aquifer with high vapor content between 100 and 200 m depth (Melosh et al., 2012). The inverted temperature gradient identified in two of the wells indicates lateral fluid flow and meteoric water infiltration. The intermediate level is characterized by a relatively constant, conductive-type gradient of 20–30 °C/km occurring in most of the wells. At ~670 m, a transition towards an almost isothermal gradient of <5 °C/km, typical of convective heat transfer regimes, is observed (Fig. 3).

Subsurface resistivity data of the Tolhuaca geothermal system has been obtained from geophysical studies using magnetotelluric (MT) and audio frequency magnetotelluric soundings (AMT) methods (Melosh et al., 2012; Melosh et al., 2010). Because the clay alteration that commonly caps geothermal reservoirs has low resistivity, MT and AMT are able to delineate such caps and, by association, the reservoir. Low resistivity at about 400 m depth occurs along the NW flank of the Tolhuaca volcano, following the trend of fumaroles and hot springs (Fig. 4). Another part of the resistivity anomaly extends to the south on the western flank of the stratovolcano. Argillic alteration mapped at the surface and in the wells confirms that argillic alteration is the primary cause of the low resistivity layer near the thermal areas (Melosh et al., 2012; Melosh et al., 2010).

3. Samples and methods

3.1. Mineral paragenesis

Drill core logging studies were performed in the Tol-1 borehole core of 1073 m depth drilled by MRP Geothermal Chile Ltda (formerly GGE Chile SpA). Forty-seven representative samples were taken for petrographic observations and fluid inclusions studies. The mineral paragenesis was determined using a combination of polarized light microscopy and scanning electron microcopy (SEM). SEM observations were performed at the Andean Geothermal Center of Excellence (CEGA), Universidad de Chile, using a FEI Quanta 250 SEM equipped with a solid-state energy dispersive X-ray spectrometer (EDS) and a cathodoluminescence (CL) detector. The mineralogical results were contrasted and complemented with previous studies of the geothermal system that include X-ray diffraction (XRD) data (Melosh et al., 2012; Melosh et al., 2010).

3.2. Borehole temperatures and fluid chemistry

Available temperature data of the four deep wells were used to constrain subsurface temperatures of the geothermal system at Tolhuaca. Water samples were collected from Tol-4 well in January 2013 using sampling procedures after Giggenbach and Goguel (1989). Samples were analyzed for major cations and anions, and trace elements at Actlabs Laboratories, Canada, using a Varian-730-ES Axial ICP-OES, a Dionex ICS-1000 ion chromatography system and a sector field HR-ICP-MS system (Thermo Element 2), respectively.

3.3. Fluid inclusion microthermometry and LA-ICP-MS analysis

Microthermometric determinations and laser ablation inductively coupled plasma mass spectrometry (LA-ICP-MS) analyses were performed in selected fluid inclusion assemblages (FIAs) hosted in quartz and calcite veins. Prior to analysis, FIAs were recognized using polarized light microscopy and SEM-based cathodoluminescence analysis in euhedral quartz crystals; FIAs correspond to groups of petrographically-associated fluid inclusions that formed simultaneously (Roedder and Bodnar, 1997).

Fluid inclusion microthermometry was performed at the Institute of Geochemistry and Petrology, ETH-Zürich, Switzerland, and at the Universidad Católica del Norte, Antofagasta, Chile, using a Linkam THMSG-600 heating-freezing stage. The stage was calibrated with synthetic fluid inclusions of pure H_2O (final ice melting temperature: 0.0 °C, homogenization temperature: 374.0 °C) and CO_2 (final CO_2 ice melting temperature: −56.6 °C). Inclusions were cooled to −196 °C to test for the presence of CO_2 or CH_4. Salinities were derived from final ice melting temperatures and are calculated as wt.% equivalent (eq.) NaCl (Bodnar, 1993). In total, 243 fluid inclusions from 48 FIAs were measured.

Chemical microanalysis of individual fluid inclusions was performed using a laser ablation system (193 nm ArF excimer laser) connected to a

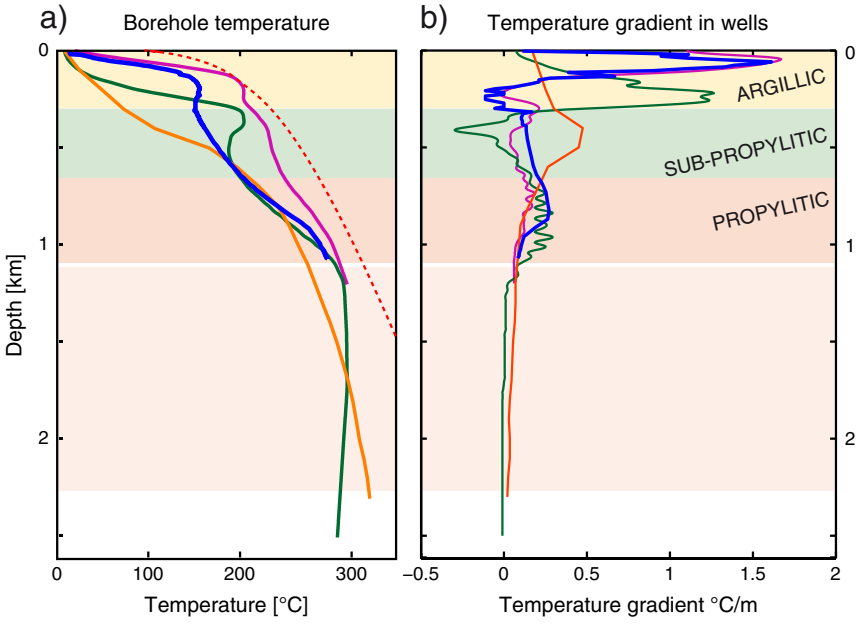

Fig. 3. Present-day temperature conditions of the Tolhuaca geothermal system. The three structural-mineralogical zones are shown as a reference. The contrasting dominant heat transfer mechanism for each zone is controlled by permeability conditions. The low permeability, clay-rich cap layer (or clay cap) is shown in light green (sub-propylitic zone) a, Temperature vs. depth profiles for the Tol-1 (blue line), Tol-2 (magenta line), Tol-3 (orange line) and Tol-4 (green line)wells. Boiling curve for pure water (dashed red line) is shown as a reference. b, Temperature gradient vs. depth profiles.

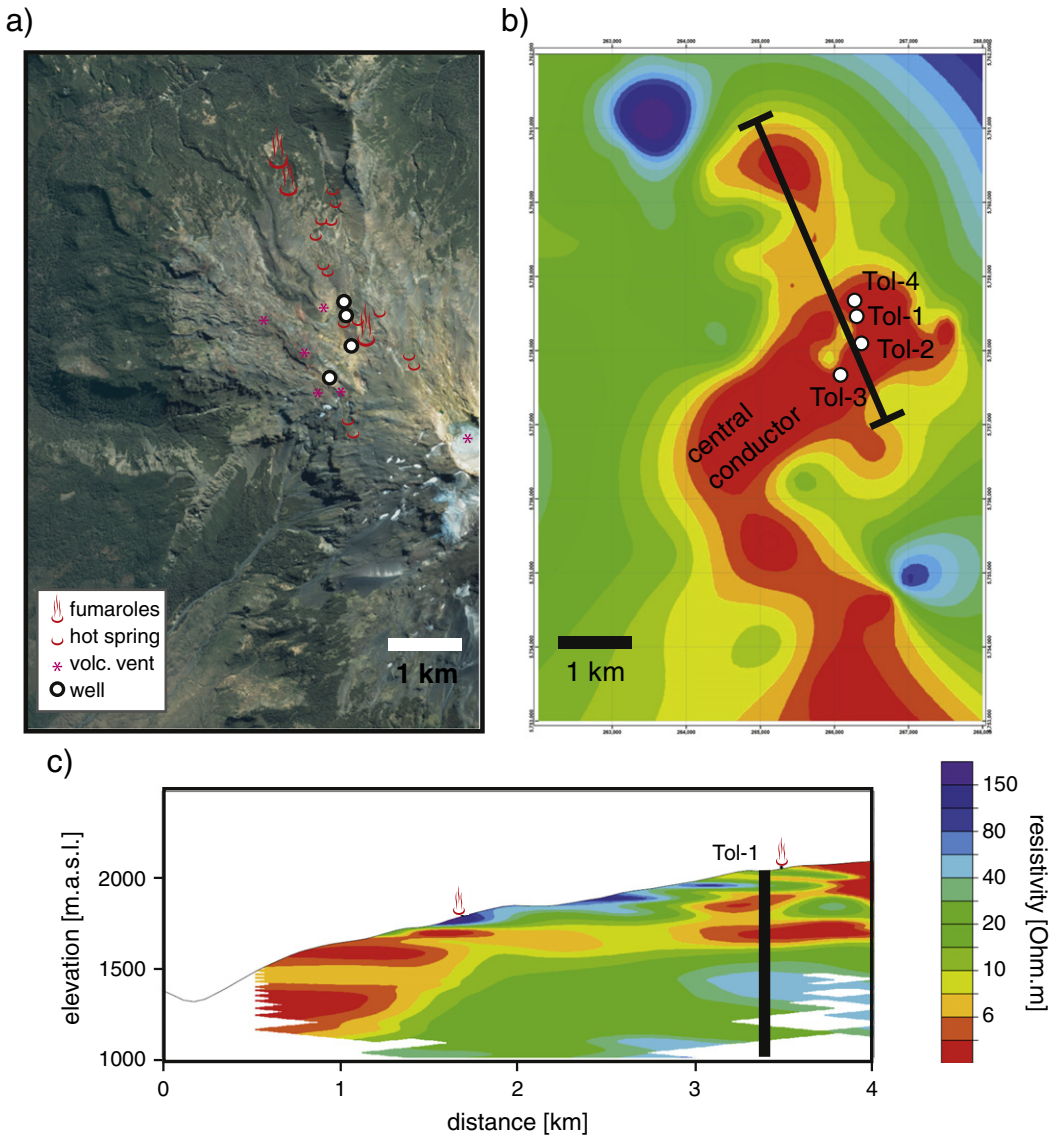

Fig. 4. Resistivity data of the Tolhuaca geothermal system obtained using magnetoteluric methods (modified from Melosh et al., 2010, 2012). a) Plan view of conductance to 400 m. The local low resistivity zone (in red) reveals the spatial distribution of the clay-rich zone. The location of the profile in c) is shown in black lines. c) Resistivity cross section along the NW flank of the Tolhuaca volcano. The well Tol-1 and fumaroles are shown for reference.

quadrupole ICP-MS (Perkin Elmer Elan 6100 DRC) at the Fluid Inclusions Laboratory in ETH-Zürich (technical details in Günther et al., 1998). As the detection limits of LA-ICP-MS microanalysis are strongly dependent on fluid inclusion size, successful analysis of low-salinity fluids required fluid inclusion sizes of at least 40–60 μm. LA-ICP-MS settings (e.g. dwell time) were optimized for the enriched components in the bore-hole fluid (e.g., B, As) and metals of interest (e.g., Cu, Zn, Au).

3.4. Rock mechanics calculation

In order to explore the effect of fluid pressure and stress states in the enhancement of permeability at Tolhuaca, the critical pore fluid pressure was calculated. In particular, the effect of a low-cohesion clay cap on the failure conditions was analyzed by considering the rock properties of two end-members, intact rock and hydrothermally altered rock with preexisting fractures. To calculate the critical pore pressure (Wiprut and Zoback, 2000) at which a fault element will begin to slip, Coulomb frictional failure was used (Secor, 1965):

$$P_f^{crit-Shear} = \sigma_n - (\tau - C)/\mu \quad (1)$$

where μ is the coefficient of sliding friction and C is cohesive strength and σ_n, τ are normal stress and shear stress respectively. To determine the critical pore pressure at which a fracture element will begin to open as an extensional fracture, the criterion for hydraulic extension was used (Secor, 1965):

$$P_f^{crit-Ext} = \sigma_n + T \quad (2)$$

where T is tensile strength.

The intact rock case considers T = 5 MPa, C = 10 MPa and μ = 0.75. The hydrothermally altered rock considers T = 1.5 MPa, C = 0.1 MPa and μ = 0.70, reflecting the decrease of tensile strength, cohesion and coefficient of sliding friction from the intact rock conditions that has been widely recognized in the hydrothermal environment (Heap

et al., 2015; Meller and Kohl, 2014; Neuzil, 1994; Tembe et al., 2010; Wyering et al., 2014).

This analysis is similar to that of Cox (2010) for exploring the roles of fluid pressure and stress states in the enhancement of permeability. However, to obtain a semi-quantitative estimation of the pressure magnitudes, we used an approximation of the stress field magnitude. The magnitude of the stress field was estimated by using a compilation of the absolute stress magnitudes measured in-situ (Zang et al., 2012). Based on kinematic analysis of fault-slip data from Tol-1 borehole that indicates a normal strain regime (Perez-Flores et al., 2013) we used the stress magnitudes compiled by Zang et al. (2012), for normal faulting regime described as:

$$Sv = 260\ \mathrm{bar/km}, S_h = 0.57S_v, S_H = 0.87S_v \quad (3)$$

where S_v, S_h and S_H are vertical, minimum horizontal and maximum horizontal stress component, respectively. Despite the fact in-situ measurements are not yet available at Tolhuaca, the magnitudes in (3) are useful as a first approximation to quantify the stress field and analyze the effect of hydrothermal alteration.

To calculate the effect of fracture orientation on the critical pore pressure that would trigger rupture, the calculations were performed in a 3D space. Thus, σ_n, τ, $P_f^{crit-Ext}$ and $P_f^{crit-Shear}$ were computed for an equidistant grid of planes in the 3D space and plotted in equal area stereonets.

3.5. Heat and fluid flow simulations

Numerical models of coupled heat transfer and fluid flow were computed using HYDROTHERM software (Hayba and Ingebritsen, 1994) to simulate the long-term effect of a low-permeability cap in the evolution of a Tolhuaca-like hydrothermal system. The system is represented in a two-dimensional symmetric geometry, where the topography and clay cap spatial distribution were set as in Tolhuaca (Melosh et al., 2012).

The modeled heat source of the system is a magma body that instantly intrudes beneath the volcano summit, as it has been widely used to analyze the evolution of hydrothermal systems (Hayba and Ingebritsen, 1997; Ingebritsen et al., 2010; Kostova et al., 2004; Scott et al., 2015; Weis et al., 2012). At Tolhuaca, the deep drilling intercepted dikes, supporting the idea of a magmatic intrusion as a heat source for the geothermal system (Melosh et al., 2012). As a first approximation, the magma body initially has a rectangular geometry with 2 km of vertical extent and a 0.5 km half width (~3 km^3) and intrudes to a depth of ~3 km at a temperature of 900 °C within a host-rock at with a temperature gradient of 20 °C/km. Repeated intrusion and/or the effect of replenishment have not been included in the simulations. Initial temperature of the magma body is a conservative value considering that lavas at Tolhuaca are mainly of basaltic andesite composition. Model characteristics, including rock properties, temperature-dependent permeability and initial and boundary conditions are similar to those used by Hayba and Ingebritsen (1997) and Scott et al. (2015).

Because rock permeability data are not available for the Tolhuaca geothermal field, the permeability input values used in our numerical simulations are equivalent to those used in similar studies (e.g. Hayba and Ingebritsen, 1997; Scott et al., 2015) which are in agreement with permeability measurements in rock samples of active hydrothermal systems (Ingebritsen and Manning, 1999, 2011). Permeability is considered as homogenous and isotropic, with values of 10^{-15} m^2 and 10^{-18} m^2 for the host rock and clay cap, respectively, within the domain of brittle rock behavior (T < 360 °C). To mimic the effect of the brittle–ductile transition, the model assumes the formulation of Hayba and Ingebritsen (1997) of temperature-dependent permeability in which permeability decreases log-linearly with increasing temperature above 360 °C (representing silicic rocks at typical crustal strain rates).

Several numerical experiments were computed to calibrate the model using the measured borehole temperature data, temperature gradients and pressure distribution, and varying intrusion depth and permeability values. In order to estimate the effect of a low-permeability clay cap in the thermal evolution of the system, selected models were analyzed with and without a clay cap.

4. Results

4.1. Mineral paragenesis

Drill core logging and petrographic observations reveal that the Tolhuaca geothermal system is characterized by a mineralogical and structural compartmentalization (Figs. 5 and 6). Three hydrothermal alteration zones were recognized: (1) a shallow argillic alteration zone (0–300 m), characterized by clay minerals (smectite, interlayered chlorite-smectite), iron oxides and stilbite; (2) an intermediate sub-propylitic alteration zone (300–670 m), dominated by widespread and pervasive occurrence of interlayered chlorite-smectite and illite; and (3) a deep propylitic zone (670–1073 m), characterized by the occurrence of epidote and chlorite. The intensity of alteration in the groundmass and phenocrysts is variable, even at thin-section scale. However, the highest intensity is observed in the shallow region (~100 m depth) near the location of the steam-heated aquifer.

Four paragenetic stages (S1, S2, S3 and S4) are recognized within the different alteration zones (Fig. 5). In the shallow argillic alteration zone (0–300 m depth), the earliest stage S1 consists of a sequence of iron-oxides (hematite), bands of amorphous silica and/or chalcedony, and late pyrite with minor chalcopyrite. The S2 stage is dominated by clay mineral assemblages including smectite, minor interlayered chlorite-smectite, and stilbite, while the S3 stage is represented by calcite with lattice-bladed texture and euhedral quartz. Finally, the S4 stage is dominated by microcrystalline quartz and amorphous silica phases.

In the intermediate sub-propylitic zone (300–670 m), the S1 stage is represented by iron-oxides followed by chalcedony bands. The S2 stage is dominated by pervasive alteration to clay minerals (interlayered chlorite-smectite), whereas the S3 stage is represented by calcite that alternates with microcrystalline quartz. Unlike the other zones, lattice-bladed texture in calcite is absent in the intermediate sub-propylitic zone. The final S4 stage is marked by the precipitation of calcite and euhedral quartz. These observations are indicative of the presence of a clay-rich cap in the upper part of the system (<670 m). The development of this intrinsically low-permeability layer is paragenetically tied to the S2 stage.

In the deep propylitic zone (>670 m), the S1 stage is represented by pyrite and chalcedony and/or microcrystalline quartz. The S2 stage consists of chlorite and epidote, while the S3 stage is characterized by the occurrence of quartz with various textures (euhedral, plumose and microcrystalline) and lattice-bladed calcite. The latest stage (S4) is marked by the occurrence of wairakite and late prehnite.

4.2. Fluid inclusion petrography, microthermometry and chemistry

Fluid inclusion petrography, microthermometry and LA-ICP-MS analyses were performed on quartz and calcite crystals from eleven veins from paragenetic stages S2, S3 and S4 comprising the three mineralogical segments. Only primary and pseudo-secondary fluid inclusions were chosen for analysis, although secondary fluid inclusion assemblages (FIAs) were measured but considered only for interpretations related to the latest alteration stage (S4). The earliest paragenetic stage S1 is characterized by complex growth patterns with scarce (and small, <5 μm) fluid inclusions, making difficult to identify reliable FIAs.

Four different types of aqueous, two-phase (liquid–vapor) fluid inclusions (FI) were identified (Fig. 7): (1) 10–30 μm sized FI hosted in massive quartz or euhedral quartz associated with stages S2 and S3 (typically oval or with negative crystal shapes), (2) 10–120 μm sized FI hosted in lattice-bladed calcite associated with stage S3 (typically with oval, elongated, or negative crystal shapes), (3) 20–100 μm sized

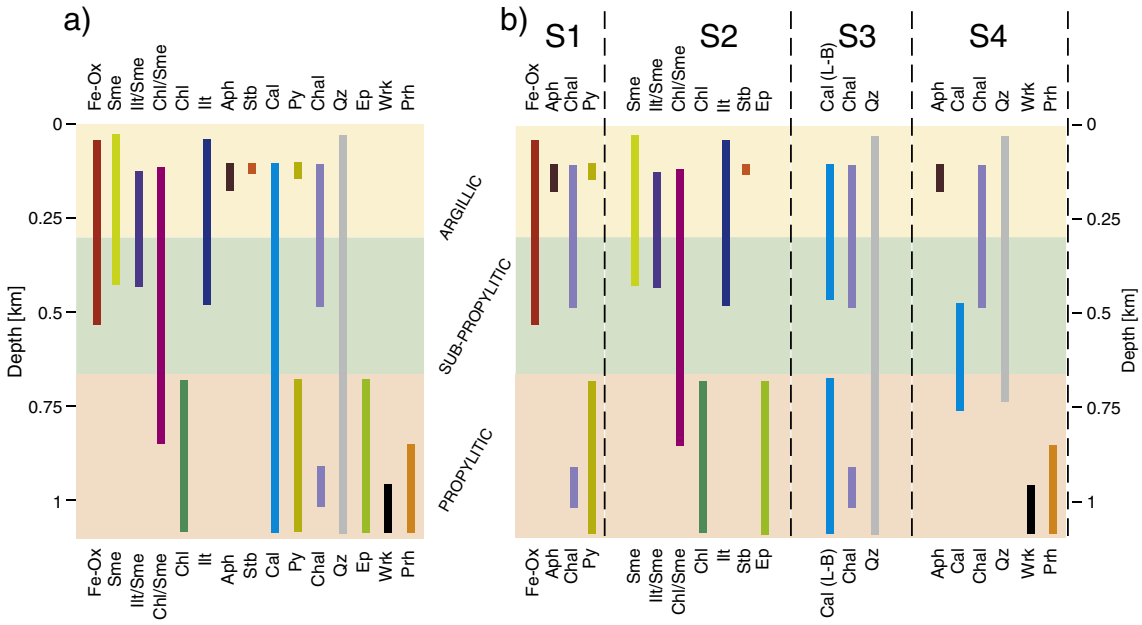

Fig. 5. a, Mineral assemblages identified in the 1073 m long Tol-1 borehole core. Three distinctive zones are recognized: argillic, sub-propylitic and propylitic. b, Paragenetic sequence considering four stages of hydrothermal alteration (S1–S4). Abbreviations are, FeOx: Iron oxides, Aph: Amourphous silica, Py: Pyrite, Chal: Chalcedony, Qz: Quartz, Chl: Chlorite, Sme: Smectite, Ilt: Illite, Stb: Stilbite, Cal: Calcite, Prh: Prehnite, Wrk: Wairakite, Ep: Epidote, (L-B): lattice-bladed texture in calcite.

FI hosted in syn-kinematic or late calcite associated with stage S4 (typically negative crystal shape), (4) pseudosecondary FI that crosscut quartz crystals, most likely trapped synchronous to prehnite precipitation. These latter FI are associated with stage S4 and are typically oval shapes with sizes between 10 and 15 μm. Most of the successful quantitative spot-analyses made by LA-ICP-MS were obtained in large (>50 μm) FI from types (2) and (3).

The average total homogenization (Th_{tot}) and final ice melting (Tm_{ice}) temperatures for each FIAs are plotted as a function of depth in Fig. 8. The temperatures of first ice melting were close to −23 °C, strongly suggesting the presence of NaCl–H_2O-dominated fluids. All fluid inclusions show final ice melting in the temperature range between −0.0 and −2.3 °C, corresponding to salinities that range from 0 to 3.8 wt.% eq. NaCl. The presence of substantial concentrations of CO_2 in the fluid inclusions is excluded because no clathrate melting was observed upon heating to room temperature. The microthermometric data show a correlation within ±40 °C between Th and present-day temperatures measured in wells (Fig. 8). The Th_{tot} data of FIAs related to the S3 stage indicate that the boiling temperature was reached, which is consistent with mineral textures such as lattice-bladed calcite. The Th_{tot} measured in FIAs related to the latest paragentic stage (S4) are similar to present borehole temperatures (Fig. 8).

The chemistry of fluid inclusions was quantified using LA-ICP-MS in fifteen out of over two hundred (206) fluid inclusions analyzed. Elements analyzed were restricted to Cu, Zn, B and As due to the small amount of sample fluid (<10 ng) contained in the small (<80 μm) and low salinity (<3 wt.% eq. NaCl) fluid inclusions at Tolhuaca. The LA-ICP-MS data are shown in Table 1 and are expressed as molar ratios rather than absolute concentrations in order to avoid the error introduced when the apparent salinity is used as internal standard, considering that the error is more relevant for low-salinity fluids. The element-to-Na molar ratios of single inclusions and the average of all FIAs are plotted along their standard deviations in Fig. 9. To the best of our knowledge these are the first quantitative chemical data of single fluid inclusions in an active geothermal system.

The quantitative results on the fluid inclusion chemistry indicate that, after Na, B is the most abundant element. B/Na and As/Na molar ratios present a slight tendency to increase with time in the different paragenetic stages. Zn/Na and Cu/Na molar ratios were measured in one paragenetic stage and therefore their chemical evolution is possible to analyze only with respect to borehole fluids. Variations with respect to depth of the elemental concentration ratios for the different FIAs are smaller than an order of magnitude and do not show a clear tendency.

4.3. Borehole fluid chemistry

The chemistry of borehole fluids at Tolhuaca was determined from aqueous samples retrieved from the Tol-4 deep geothermal well during a flow test. The main chemical features of the liquid phase are low salinity (Na = 178 mg/kg; Cl = 266 mg/kg) and sulfur contents (SO_4 = 8.7 mg/kg), and relatively high concentrations of metals including Au (1.57 μg/kg), Ag (0.018 μg/kg), Cu (0.07 μg/kg) and Zn (7.5 μg/kg). Boron (219 mg/kg) and As (25.6 mg/kg) contents are particularly high. The measured concentration of other components in the liquid phase is Si = 234, K = 39.1, Ca = 1.8, Al = 1, Li = 1.2 and Mg < 0.1 in mg/kg of water.

In Fig. 9 and Table 1, borehole fluid chemistry is compared with the quantitative measurements in fluid inclusions. These results show that fluid inclusions (paleofluids) and borehole (present-day) fluids at Tolhuaca are significantly different in terms of chemical composition. While borehole fluids are rich in Au, B and As, but Cu-poor (B/Na ~ $10^{0.5}$, As/Na ~ $10^{-1.1}$, Cu/Na ~ $10^{-4.2}$), the paleofluids trapped in fluid inclusions are Cu-rich but poor in B and As (B/Na ~ 10^{-1}, As/Na ~ $10^{-2.5}$, Cu/Na ~ $10^{-2.5}$ in average) (Fig. 9).

5. Discussion

5.1. Development of vertical compartmentalization at Tolhuaca

The mineralogical analysis of samples retrieved from the Tol-1 drillcore revealed the presence of four stages of hydrothermal alteration during the lifespan of the Tolhuaca geothermal system, in agreement with previous studies in the area (Melosh et al., 2012; Melosh et al., 2010). The S1 stage represents the early heating event characterized by precipitation of iron-oxides, quartz and chalcedony. The ubiquitous co-precipitation of silica phases and the formation of hydrothermal breccias at the end of the S1 are indicative of widespread boiling and flashing conditions, suggesting a catastrophic event (Moncada et al.,

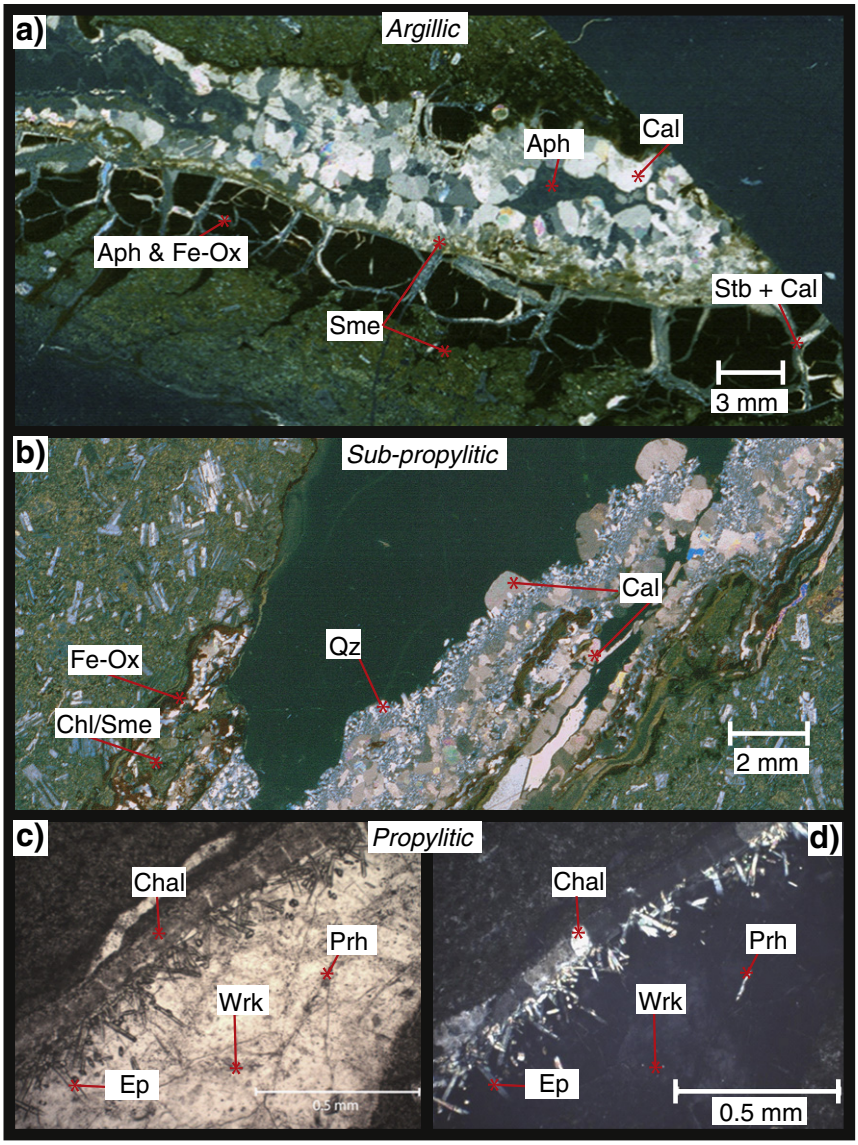

Fig. 6. Photomicrographs of representative samples taken from the three hydrothermal alteration zones. Plane-polarized light for a), b) and c); crossed-polarized light for d). Abbreviation of minerals is same to Fig. 3. *(a) Argillic Zone (104 m).* Early amorphous silica bands with colloform texture interlayered with iron oxides, cut by two-direction-cleavage-zeolite and calcite micro veins (<0.5 mm) forming a mineral breccia texture. Pyrite and chalcopyrite occurrence is restricted to the amorphous silica and iron oxide bands. A yellowish green halo of interlayered clay minerals (chl/sme) forms towards the main vein up to the brecciated outer part. In the inner part, the later stages are represented by bladed calcite and late amorphous silica with moss texture unaffected by clay alteration. *(b) Sub-Propylitic Zone (410.6 m).* Chalcedony bands, iron oxides and interlayered clay minerals (chl/sme). Calcite and quartz with different textures alternate in the inner part of the vein. The size of quartz crystals increases towards the center of the vein, from microcrystalline to euhedral. *(c) & (d) Propylitic Zone (947.8 m).* A chalcedony band (outer rim) is followed, towards the center of the vein, by prismatic euhedral epidote and wairakite. The main vein is cut obliquely by micro-veins of prehnite.

2012). We propose that such event caused brecciation and flashing conditions at the end of stage S1, and might have been related to depressurization as a result of glacial retreat during the late Pleistocene and/or flank collapse, as proposed for the Karaha-Telaga Bodas geothermal systems in Indonesia (Moore et al., 2008).

The S2 stage represents an episode of pervasive hydrothermal circulation and alteration of volcanic and volcaniclastic rocks to form the typical mineral assemblages of geothermal systems related to magmatic activity: an argillic assemblage consisting of illite, smectite, chlorite, calcite, and silica (chalcedony) at shallow depths and on the periphery of the system; and a propylitic assemblage consisting of quartz, K-feldspar, albite, illite, chlorite, pyrite, epidote and calcite within the deep central upflow zone (Browne, 1978; Simmons and Browne, 2000). Our data suggest that the S2 stage marks the beginning of the mineralogical, hydrological and structural vertical compartmentalization of the geothermal system at Tolhuaca. It is likely that this segmentation was the result of fluctuating physical and chemical conditions at the reservoir, mostly controlled by heat-fluid–rock interaction processes. A key controlling factor was the maximum temperature achieved at geothermal reservoir conditions, which is commonly limited by liquid-saturated conditions. Under such conditions, low temperature (<200 °C) argillic alteration assemblages (smectite; illite/smectite; interlayered chlorite/smectite, calcite and chalcedony/amorphous silica) were developed during the S2 stage in the shallower levels of the system (<670 m), as commonly recognized in geothermal fields (e.g. Simmons and Browne, 2000). In contrast, propylitic alteration assemblages with chlorite, epidote, quartz, calcite and pyrite were formed in the deep upflow zone (>700 m), under higher temperature (≥250 °C) and near-neutral, rock-buffered fluid conditions.

The S3 stage reflects processes occurring within a highly compartmentalized system. In the argillic zone, calcite with lattice-bladed texture, quartz with plumose texture and the coexistence of silica phases

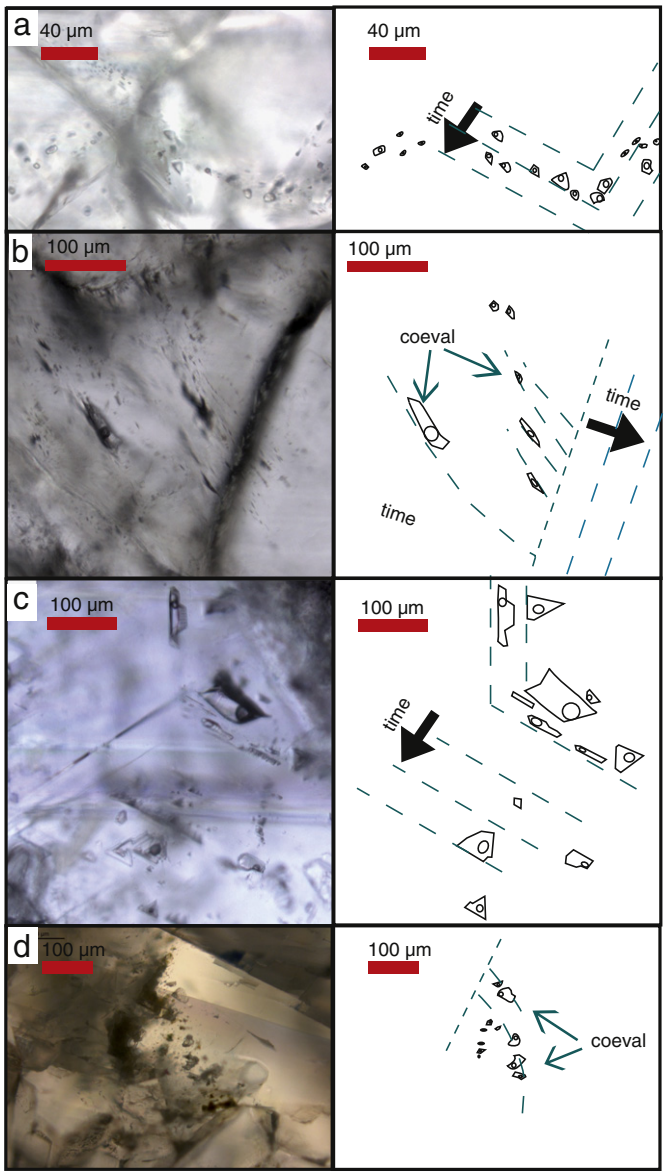

Fig. 7. Fluid inclusion assemblages (FIAs) types at Tolhuaca. a, Fluid inclusions hosted in euhedral quartz associated with the S3 stage. b, Fluid inclusions hosted in lattice-bladed calcite (S3 stage). c, Fluid inclusions hosted in syn-kinematic calcite associated with the S4 stage. d, Pseudo-secondary fluid inclusions that crosscut quartz crystals associated with the S4 stage.

with variable degrees of crystallinity are indicative of boiling and flashing which is most likely related to the formation of the steam-heated aquifer at the top of the system. Brecciation also occurs in the deep propylitic zone, suggesting transient changes in the physical conditions triggering fault rupture during the development of the geothermal reservoir at liquid-saturated conditions. The homogenization temperature data from FIAs related to the S3 stage supports such interpretation and point to boiling in the upper and lower zones of the system. Unlike the other two zones, evidence of boiling such as lattice-bladed calcite is absent in the sub-propylitic zone. Finally, the S4 stage reveals a gentler phase of fluid mixing and boiling. In the sub-propylitic zone, the homogenization temperature data of fluid inclusions is approximately 50 °C less than the boiling temperature for the corresponding depth, coinciding with the present-day borehole temperature conditions. In the deep propylitic zone, localized prehnite after epidote may suggest a cooling event as previously proposed by Melosh et al. (2012). However, homogenization temperature data related to stages S3 and S4 are similar to present-day borehole temperatures (Fig. 8), ruling out an episode of widespread and significant cooling.

The heat transfer regime has also been affected by the vertical compartmentalization at Tolhuaca, as revealed by the contrasting vertical temperature gradients shown in Fig. 3. Convection dominates in the propylitic zone, whereas in the sub-propylitic zone the constant gradient indicates a conductive heat transfer regime. The vapor phase, formed in the boiling reservoir, is capable to migrate through the low-permeability clay cap, reaching the meteoric water level and forming a steam-heated aquifer in the argillic zone. Within this zone, lateral fluid flow and meteoric water infiltration is favored by the presence of open fractures, as indicated by the inverse temperature change and localized large temperature changes. It is relevant to note that homogenization temperature data from fluid inclusions of all alteration stages and depths are within a range of ±40 °C from present-day borehole temperatures and show a similar temperature gradient. These data suggest that temperature did not fluctuate significantly after the early heating stage (S1).

5.2. Chemical evolution of fluids

The geochemical analyses of fluid samples retrieved from the Tol-4 deep well indicate that present-day fluids are neutral chloride geothermal fluids with low salinity and relatively high content of metals (Table 1 and Fig. 9). Those are common features in active geothermal systems and low-sulphidation epithermal environments (Simmons et al., 2005). The high B and As contents are likely supplied by a magmatic-vapor contribution (Pokrovski et al., 2013). Such interpretation is supported by helium isotope data with a mantle-like signature from fumaroles ($He^3/He^4 = 6.5$ Ra) (Dobson et al., 2013).

The comparison between (present-day) borehole fluids and fluid inclusion data reveals significant differences. Fluid inclusions are Cu-rich but poor in B and As while borehole fluids are rich in Au, B and As, but Cu-poor (Fig. 9). Simple boiling models cannot explain the aforementioned differences in fluid chemistry because liquid-phase molal ratios of non-volatiles such as Cu/Na, B/Na and As/Na are almost unaffected during simple boiling. These non-volatile elements remain in the liquid phase during boiling as revealed by their liquid–vapor partitioning coefficients ($K_d = C_{vapor}/C_{liquid}$, B = 0.001–0.1; As = 0.001–0.01; Cu < 10^{-3}; Na < 10^{-3}) at epithermal conditions (100 < T < 280 °C, P_{sat}; Pokrovski et al., 2013).

These data are in agreement with recent mineralogical studies documenting abrupt chemical and isotopic changes recorded in hydrothermal sulfides from epithermal Au systems (Deditius et al., 2009; Peterson and Mavrogenes, 2014) and porphyry Cu(Au) deposits (Reich et al., 2013). The oscillatory chemical zonations reported in pyrite from such deposits are indicative of geochemical decoupling of As and Cu, where Cu-rich, As-poor bands alternate with As-rich, Cu-poor bands. Moreover, significant changes in the trace-element and sulfur-isotope signatures in pyrite have been interpreted by Peterson and Mavrogenes (2014) as the result of fluid chemistry changes driven by transient pressure drops due to fault failure. Therefore, we interpret the fluctuations in fluid chemistry at Tolhuaca as the result of transient supply of metal-rich, magmatically derived fluids where As, Au and Cu are geochemically decoupled, and most likely driven by fault/fracture activity.

5.3. Effects of hydrothermal alteration on the physical evolution of the system

Results presented in this study suggest that during the early stages of evolution at Tolhuaca, the development of a clay-rich zone may have affected the mechanical properties of the rock leading to the development of a mineralogical, hydrological and structural vertical segmentation. Moreover, fluctuations in fluid chemistry suggest that fluid source and/or pressure and temperature conditions have varied significantly

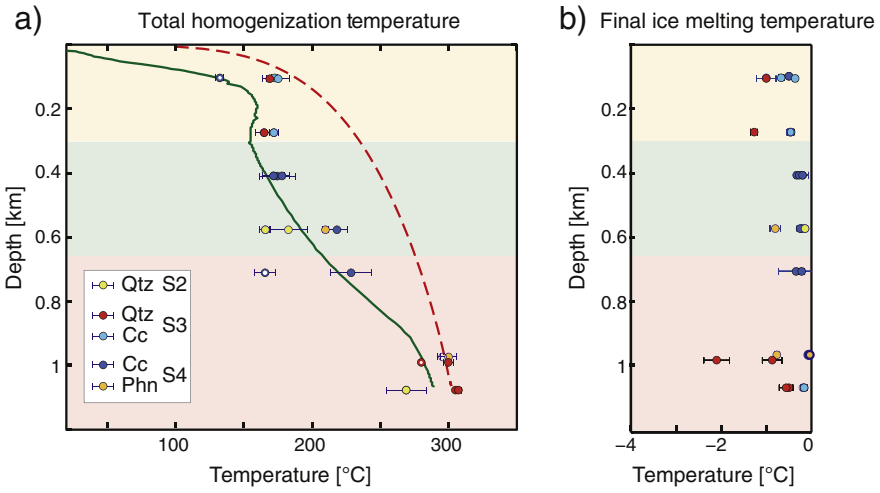

Fig. 8. Paleo-fluid temperature (a) and apparent salinity (b) conditions determined by microthermometry measurements. Solid circles show the average homogenization and final ice melting temperatures of FIAs. Error bars indicate 1-sigma standard deviation and colors depict the paragenetic stage. The boiling temperature as a function of depth for pure water (dashed red line) and present-day borehole temperature of the Tol-1 well (green line) are shown. Background colors represent the structural-mineralogical zones.

during the evolution of the Tolhuaca geothermal system. Because mineralogical, mechanical and chemical variations are known to significantly affect the evolution of high enthalpy systems (Davatzes and Hickman, 2010; Meller and Kohl, 2014; Nemcok et al., 2004), in the next section we aim at evaluating the feedbacks between hydrothermal alteration and brittle deformation at Tolhuaca by performing semi-quantitative rock mechanics calculations. We first performed fault-rupture calculations to evaluate the effect of a clay-rich level on the likelihood of forming or reactivating highly permeable fractures. Secondly, we analyze the effect of a low permeability, clay-rich zone on the long term pressure and temperature evolution of the Tolhuaca system.

5.3.1. Calculations of fault rupture conditions

To assess the effects of hydrothermal alteration on faulting conditions we calculated the critical fluid pressures (P_f^{crit}) that would trigger rupture on faults (Wiprut and Zoback, 2000) by combining mesoscopic failure criteria with estimation of the stress field in the Tolhuaca area. The minimum and maximum fluid pressure required to rupture extensional and shear faults were calculated considering two different scenarios. The first scenario considers intact rock conditions while second scenario takes into account the effect of hydrothermal alteration in a clay-rich rock with preexisting fractures. The intact rock conditions are likely to mimic the reservoir host rocks in the propylitic alteration zone (Fig. 5) where the precipitation of calcite and quartz has helped retain brittle dilatant behavior (Davatzes and Hickman, 2010). The scenario considering a hydrothermally altered clay-rich rock mimics the ductile behavior occurring in the sub-propylitic alteration zone (Fig. 5). The minimum calculated fluid pressure required for faulting corresponds to rupture on optimally oriented planes. In contrast, the maximum fluid pressure to rupture is required for the severely misoriented planes. We assume that the stress conditions of an extensional regime are representative of the stress field at Tolhuaca based on kinematic analysis of fault-slip data from Tol-1 borehole that indicates a N60°E-striking bulk fault plane solution with a normal strain regime (Perez-Flores et al., 2013). Therefore, our calculations use the stress magnitudes compiled by Zang et al. (2012) for a normal faulting end-member and a direction of the maximum horizontal stress component (S_H) of N60°E, consistent with the kinematic analysis of Tol-1 (Perez-Flores et al., 2013, Perez-Flores et al., *in prep*).

Calculations of the maximum and minimum P_f^{crit} for the two scenarios are shown in Fig. 10. For the intact-rock scenario, extensional fractures require less fluid pressure to rupture than shear faults within shallower depth levels (~2 km) (Fig. 10a). At greater depths (i.e., higher differential stress and confining pressure), shear failure requires lower fluid pressures (Fig. 10a). In contrast, for the hydrothermally altered rock scenario, cohesionless fractures are present and

Table 1
Fluid chemistry data from LA-ICP-MS microanalysis of fluid inclusions. Data is normalized to Na in molal ratios to avoid error introduced by internal standards. b.d.: below detection limit. The chemical composition of a sample retrieved from the Tol-4 deep well is also shown as a reference (bottom).

Fluid Inclusion Assemblage	Depth	Paragenetic Stage	$^{11}B/^{23}Na$	$^{65}Cu/^{23}Na$	$^{66}Zn/^{23}Na$	$^{75}As/^{23}Na$
2V-C10	99.29	S4	2.14E-01	b.d.	b.d.	b.d.
4A-CP1	106.61	S3	1.54E-01	b.d.	b.d.	1.60E-03
4A-CP1	106.61	S3	2.18E-02	b.d.	b.d.	b.d.
13A-CP2	274.85	S3	2.47E-01	b.d.	b.d.	b.d.
13A-CP2	274.85	S3	1.96E-01	b.d.	b.d.	b.d.
13A-CP2	274.85	S3	1.88E-01	b.d.	b.d.	b.d.
45Y-C4	1078.8	S4	1.58E-01	b.d.	1.43E-01	8.92E-03
20E-CK8	409.96	S4	8.00E-03	3.88E-03	1.46E-02	b.d.
20E-CK8	409.96	S4	3.16E-02	b.d.	b.d.	b.d.
19A-CK8	410.6	S4	3.17E-01	2.53E-03	5.95E-03	2.03E-03
19A-CK8	410.6	S4	2.60E-01	b.d.	b.d.	b.d.
19A-CK8	410.6	S4	1.42E-01	b.d.	b.d.	b.d.
19A-CK8	410.6	S4	8.38E-01	b.d.	b.d.	b.d.
19A-CK8	410.6	S4	1.25E+00	b.d.	b.d.	b.d.
24E-QT6	578.26	S2	3.43E-02	b.d.	b.d.	b.d.
Well (borehole Tol-4)			4.45E+00	5.49E-05	4.12E-02	5.62E-02

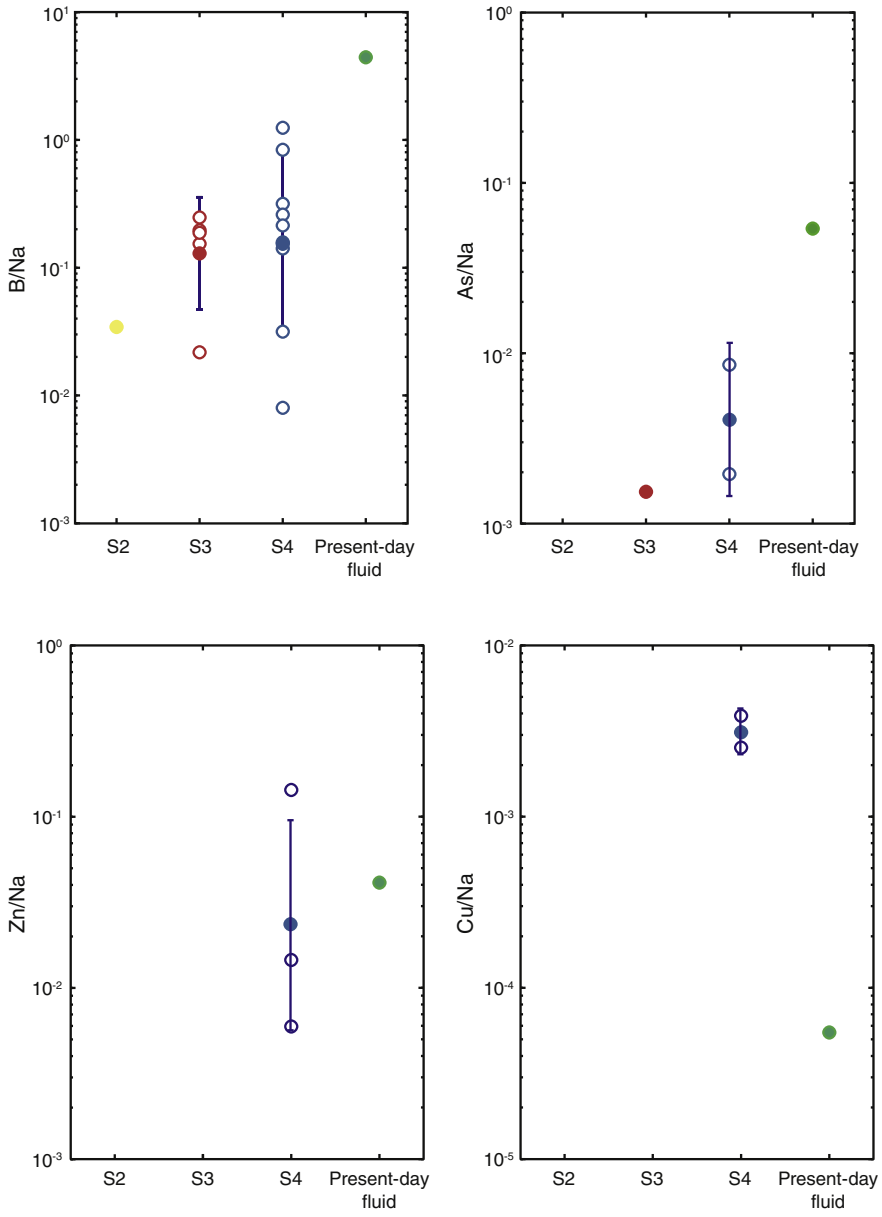

Fig. 9. Past (FIAs) and present-day (borehole fluid) fluid chemistry evolution for selected elements in molal ratios normalized to sodium. The horizontal axes display the different stages of the paragenetical sequence linked to the FIAs. Solid circles show the mean molal ratios for measured FIAs, whereas open circles are single-inclusion data. The green solid circles show present-day fluid chemistry.

thus shear failure rupture for an optimally oriented preexisting fracture requires significantly lower fluid pressure than extensional fractures at any depth (Fig. 10c,d).

This analysis estimates the effect that hydrothermal alteration has on the fluid pressure required to create or reactivate extensional and shearing fractures. In the clay cap, the lower fluid pressure required to shear cohesionless faults optimally oriented for reactivation precludes of other forms of brittle failure, such as extensional fractures. Therefore, the permeability-reducing effect of clay minerals (permeabilities of 10^{-23}–10^{-17} m^2; Neuzil, 1994) that has affected the clay-rich sub-propylitic zone at Tolhuaca is sustained by inhibition of highly permeable extensional fractures (Fig. 10). This calculation is in agreement with the high frequency of faults relative to fractures documented in the sub-propylitic zone of the Tol-1 well (Fig. 2). Moreover, the conductive heat transfer in the sub-propylitic zone, revealed both by the present-day temperature gradient (Fig. 3) and fluid inclusion homogenization temperatures (Fig. 8), suggests that the effects of hydrothermal alteration on rock mechanics have played a role on the long-term temperature and pressure evolution of the system, by sustaining the clay-rich cap.

In contrast, the less pervasive occurrence of clay minerals and precipitation of calcite and silica in other zones helps retain rock strength and brittle dilatant behavior during slip (Davatzes and Hickman, 2010; Meller and Kohl, 2014; Wyering et al., 2014). It has been shown that shear faults in rocks with brittle behavior are hydraulically conductive and help increase permeability by either sustaining fault aperture and/or producing damage zones (Barton et al., 1995; Kim, 2004). Therefore, our calculations on the fluid pressure required to rupture faults and fractures indicate that mineralogical characteristics of the deep propylitic zone at Tolhuaca promote the creation of hydraulically conductive fractures, allowing permeability regeneration and maintaining the conditions required for fluid advection (permeabilities > 10^{-16} m^2).

The dependence of P_f^{crit} on the orientation of the fracture plane is depicted for three representative depths (0.2, 0.5 and 1.1 km) of the

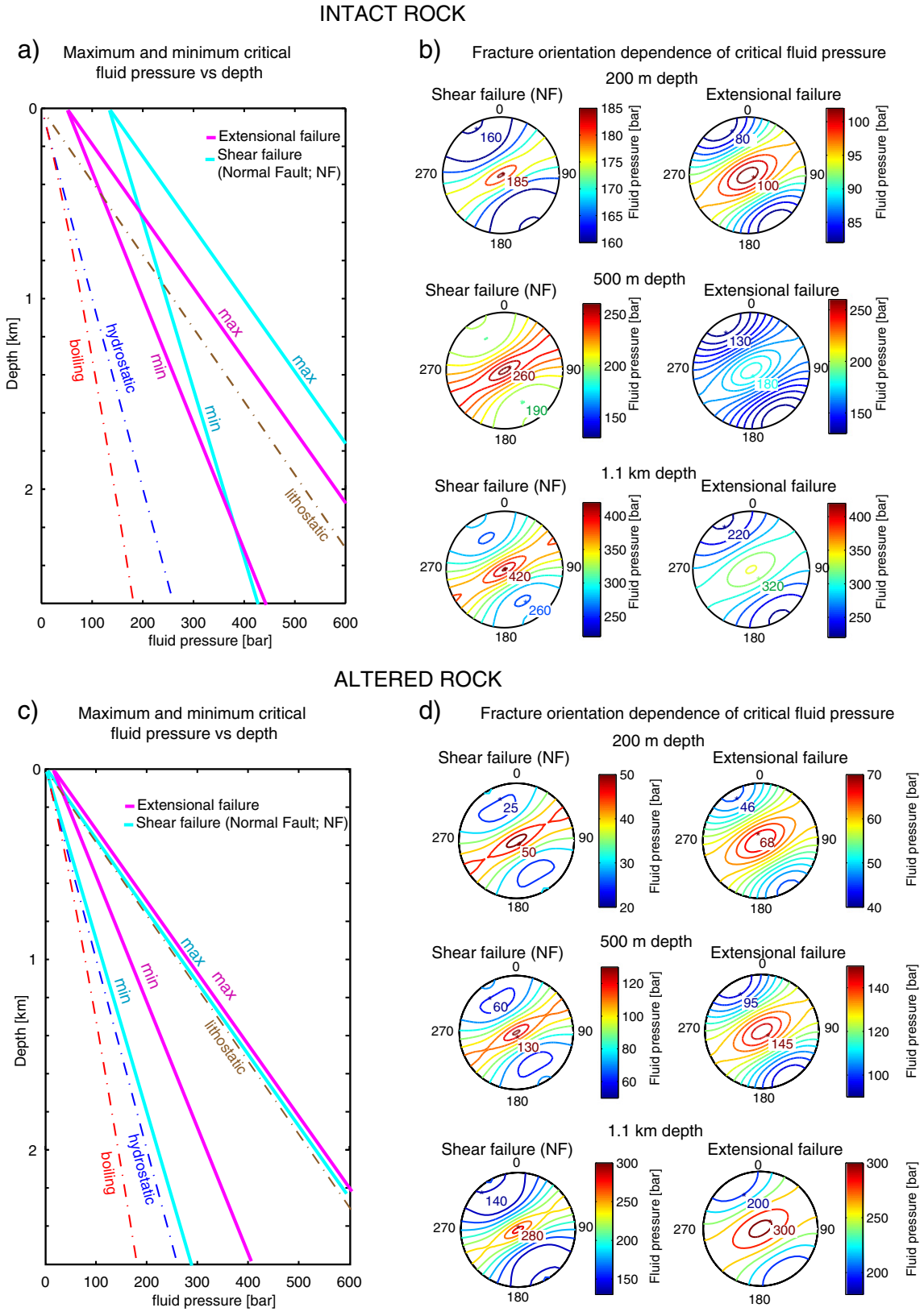

Fig. 10. Critical pore fluid pressures that trigger fault rupture (P_f^{crit}) considering intact and hydrothermally altered rock scenarios. Calculations consider shear and extensional failure modes in a normal-faulting stress regime. a, Dependence of the maximum (optimally oriented plane) and minimum (severely misoriented plane) critical P_f^{crit} on depth (km) for the intact rock scenario. Boiling, hydrostatic and lithostatic fluid pressure gradients are shown as a reference. b, Lower-hemisphere stereographic projection shows the dependence of P_f^{crit} on orientation for 200 m, 500 m and 1.1 km depths (fluid pressure in bars). The contour lines are obtained from the values of P_f^{crit} for the poles of all the existing planes. Note that the contour lines reveal the geometry of optimally oriented and severely misoriented planes for rupturing. Panels c and d are equivalent to a and b, respectively, but for the hydrothermally-altered rock case-scenario.

alteration zones in a lower-hemisphere stereographic projection (Fig. 10). The distribution and elongation of the contour lines of P_f^{crit} reflect the direction of S_H. The difference of P_f^{crit} between the optimally oriented and the severely misoriented fracture planes increases significantly with depth. Therefore, at shallow depth (<300 m), where difference is small, the two rupture types occur in a wide range of orientations. At a greater depth, a small deviation from the optimal orientation produces a larger increase on the critical fluid pressure required for rupture (P_f^{crit}), and therefore faults/fractures are likely to be nearer the optimal orientation. If fluid pressure exceeds the threshold condition required to rupture a severely misoriented extensional fracture, a breccia is formed. However, it is likely that breccias form before this limiting condition is reached. At depths of more than 2 km for intact rocks, shear rupture requires lower fluid pressures than extensional rupture. Such a limiting condition for extensional fractures may have an effect on the maximum depth of highly permeable regions for the epithermal environment.

The interplay between hydrothermal alteration and fault kinematics has been interpreted in a similar way in other active geothermal systems. For example, seismologic data and geomechanical observations at the geothermal site of Soultz-sous-Forêts in France indicate that hydrothermal alteration affects seismic activity by reducing the frictional strength of the reservoir rock (Meller and Kohl, 2014). Meller and Kohl (2014) show that on a reservoir scale, large magnitude seismic events are restricted to unaltered granites, whereas in clay-rich zones, only small magnitudes are observed. Therefore, clay rich zones foster the occurrence of aseismic movements on fractures. Structural and mineralogical observations at the volcanic-hosted Karaha–Telaga Bodas geothermal field in Indonesia, show that the clay cap is characterized by strike-slip and normal faults and tensile fractures, while the reservoir shows only tensile fractures and normal faults (Nemcok et al., 2004; Nemčok et al., 2007). Moreover, the depth at which there is a change in fault kinematics corresponds approximately to the first appearance of epidote (Nemčok et al., 2007). As at Tolhuaca, conductive temperature profiles characterize the cap rock at Karaha–Telaga Bodas, whereas the reservoir is characterized by convective profiles.

5.3.2. Effects of the clay cap on thermal structure: numerical simulations

In order to explore the effect of a low-permeability clay cap on the physical evolution of the Tolhuaca geothermal system, we performed numerical simulations of coupled heat and fluid flow using HYDROTHERM (Hayba and Ingebritsen, 1994). The modeled heat source of the system is a magma body that instantly intrudes to a depth of ~3 km beneath the volcano summit. Model geometry and initial conditions are depicted in Fig. 11. Two scenarios were considered, namely, with and without the presence of a low-permeability clay cap. In both scenarios, the intrusion of a shallow (~3 km) magma body results in an increase in enthalpy of the fluid and a decrease in fluid pressures as a result of a transition from the hydrostatic pressure gradient to a liquid-saturated (boiling) environment at reservoir depths (>670 m).

The main differences caused by the presence of a low-permeability layer or clay cap are depicted in temperature and vapor-fraction evolution in Fig. 12. In the absence of a clay cap, boiling conditions (maximum temperature for depth) are restricted to the deep part of the reservoir (>1.1 km) after 10 ka, and only occur for a short period of time (~3 ka). In contrast, in the presence of a clay cap the reservoir heats up faster and reaches boiling conditions (flat and constant temperature) near 5 ka at shallower reservoir depths (~0.9–2 km) and vapor fractions of up to 15 vol.%. Boiling conditions are sustained for a longer period of time (~10 ka) before disappearing after 15 ka.

Therefore, the presence of a low permeability clay cap increases the duration of vapor-saturated conditions (boiling temperatures) by a factor of three at the Tolhuaca reservoir depth (propylitic zone) and significantly extends the lifespan of the hydrothermal system. Our simulations indicate that such effects are mainly produced by the barrier effect that the low-permeability layer has on cold meteoric water down-flow. As in high relief regions the driving force for meteoric water down-flow increases, the effect of a low-permeability layer is likely to be enhanced in hydrothermal systems that develop near the flank of stratovolcanoes, compared to flat areas.

5.4. Conceptual model of the Tolhuaca geothermal system

The main features - including lithology, faults and isotherms - of the Tolhuaca geothermal system are shown in Fig. 13. A liquid-dominated geothermal reservoir that reaches ~300 °C occurs bellow the clay cap. In the upper limit of the reservoir, boiling conditions are reached, producing the vapor phase that feeds fumaroles and the shallow steam heated aquifer. In the reservoir, focused fluid flow is likely to be restricted to highly fractured damage zones near faults, whereas distributed fluid flow occurs in the less fractured regions. High permeability conditions are produced by fault and fracture networks that are optimally oriented for slip and dilation. Such highly permeable fault and fractures networks are likely to be genetically related to the N60°E-striking subsidiary faults of the LOFS. Resistivity data also reveals a NE-striking anomaly that may be related to highly permeable conduits (Fig. 4). High productivity wells may be related to these structural elements, and therefore identifying such structures is essential when defining drilling targets for geothermal exploration.

The development of a low-permeability clay cap at relatively shallow depths produces hydraulic compartmentalization of the system, disconnecting the deep reservoir from surface. The vapor phase is able to pass through this barrier to form the steam heated aquifer and fumaroles. Basement crystalline rocks are likely to behave as barriers for fluid flow and may act as the lower limit for large scale hydrothermal convection. Recharge fluids may be supplied by infiltration of meteoric water from the flanks of the Tolhuaca volcano and water melted from surrounding glaciers.

The presence of faults is likely to produce heterogeneities in permeability and compartmentalize fluid flow, developing convection cells limited vertically by the clay cap and laterally by the extent of high permeability conduits (Fig. 13), as it has been proposed for other active geothermal systems (Davatzes and Hickman, 2010; Nemčok et al., 2007; Rowland and Sibson, 2004).

6. Concluding remarks

Based on mineralogical observations, analysis of fluid inclusions and borehole data, we recognized four stages (S1–S4) of progressive hydrothermal alteration at Tolhuaca geothermal system. An early heating event (S1) was followed by formation of a clay-rich cap in the upper zone (<670 m) and development of a propylitic alteration assemblage at greater depth (S2). Boiling, flashing and brecciation occurred later (S3), followed by a final phase of fluid mixing and boiling (S4). Therefore, the evolution of hydrothermal alteration at Tolhuaca has produced a mineralogical, hydrological and structural segmentation of the system through the development of three alteration zones: shallow argillic; an intermediate clay-rich sub-propylitic zone; and a deep propylitic zone.

Quantitative chemical analyses of fluid inclusions and bore-hole fluids indicate that hydrothermal fluid chemistry changed significantly during the evolution of the Tolhuaca system. We interpret these fluid chemistry fluctuations as consequences of episodic supply of metal-rich hydrothermal fluids where As, Au and Cu are geochemically decoupled.

Our rock mechanic calculations indicate that the development of a low-cohesion clay-rich zone due to hydrothermal alteration has also affected faulting mechanisms. In the clay-rich region, favorable conditions for reactivation of low-cohesion preexisting faults inhibit the creation or reopening of highly permeable extension fractures. In contrast, in the deep upflow zone the less pervasive occurrence of clay mineral assemblages has helped retain rock strength and dilatant behavior during slip, contributing to sustaining permeability.

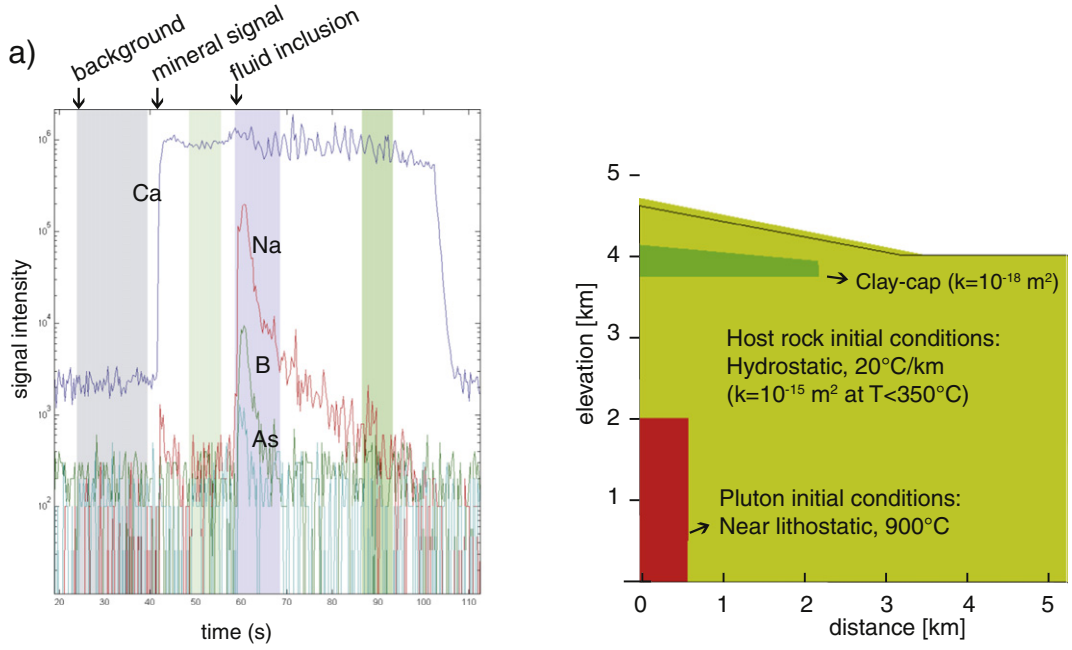

Fig. 11. Geometry and initial conditions of the numerical model of coupled heat and fluid flow computed using HYDROTHERM. Model characteristics are similar to those used by Hayba and Ingebritsen (1997). Topography and clay cap spatial distribution were set as in Tolhuaca.

Moreover, our numerical simulations of coupled heat and fluid flow indicate that the development of a low-permeability clay cap at shallow levels has modified the evolution of temperature and pressure conditions. Indeed, our numerical experiments suggest that the clay cap can increase the duration of vapor-saturated conditions (boiling temperatures) at the Tolhuaca reservoir by a factor of three, extending the lifetime of the hydrothermal system.

Finally, our results show that favorable conditions leading to the development of high enthalpy geothermal resources in the southern Andes of Chile result from the interplay between crustal brittle deformation and heat–fluid–rock interaction. The optimal alignment of such interacting processes can help sustain the magmatic heat source, enhance secondary permeability for fluid flow, and provide the conditions necessary to develop an insulating clay cap that extends the life of the geothermal system.

Acknowledgments

We acknowledge support from FONDECYT grant #1130030, CEGA-FONDAP project #15090013, and Millennium Science Initiative grant NC130065. We thank MRP-Chile Ltd. and former GGE Ltd., in particular S. Iriarte, S. Lohmar, G. Melosh, J. Stimac and A. Colvin for providing

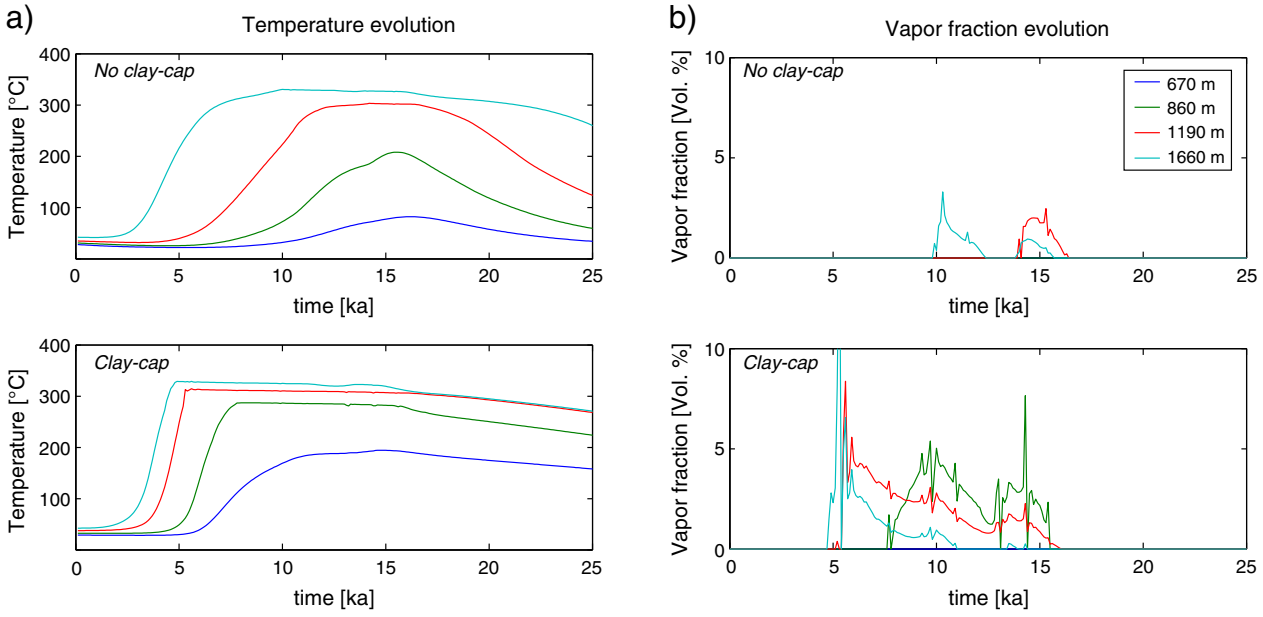

Fig. 12. Evolution of temperature (°C) and vapor (vol%) fraction as a function of time (ka) simulated for a Tolhuaca-like system under two scenarios, namely, with and without a low-permeability clay cap. Four selected depths (colored) depict the thermal structure in the vertical axis. a, Temperature evolution. An almost constant and flat temperature profile marks two-phase fluid conditions (boiling). b, Volumetric vapor fraction. Values above 0% indicate two-phase fluid conditions. Temperature and two-phase fluid conditions are maximized in duration and vertical extension when a clay cap is present.

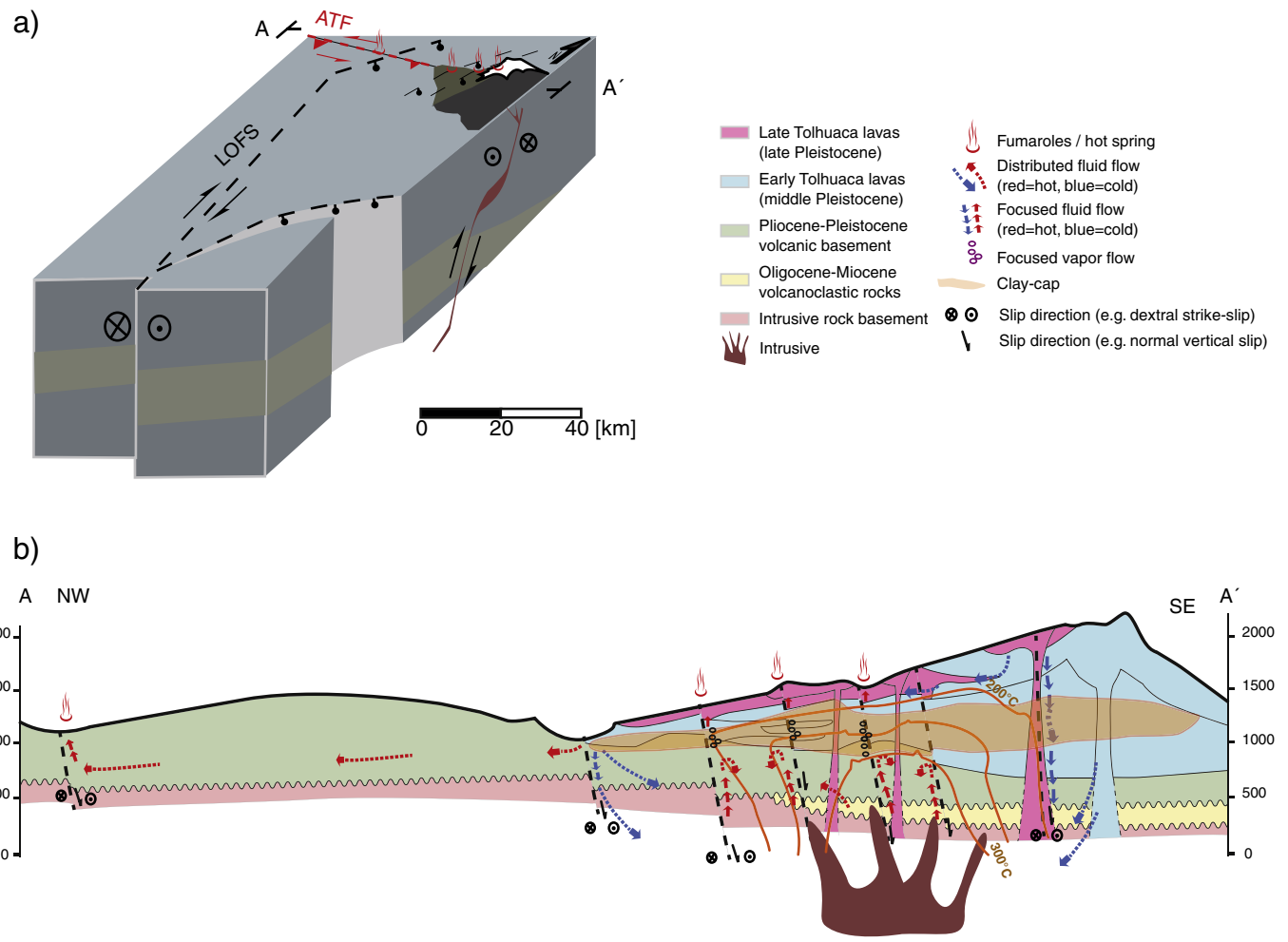

Fig. 13. Conceptual model of the Tolhuaca geothermal system at regional and local scales a, Block model showing the context of the Tolhuaca volcano in relation to the long-lived NW-trending Andean Transverse Faults (ATF) and the LOFS. b, Main features of the Tolhuaca geothermal system. Focused fluid flow is likely restricted to highly damaged zones near faults, whereas distributed flow occurs in intact rock and propylitic zones. Such heterogeneities develop convection cells limited laterally by the extent of high permeability conduits and vertically by the clay cap.

access to Tolhuaca and for information and samples used in this study. M. Wälle, S. Scott and M. Steele-MacInnis from IGP-ETH Zürich are thanked for their help during LA-ICP-MS data acquisition at ETH-Zürich. P.S., D.T. and P.P. acknowledge financial support given by MECESUP and CONICYT doctoral grants. J.C. thanks the National Research Centre for Integrated Natural Disasters Management (RCINDIM). We sincerely thank Editor in-Chief Alessandro Aiuppa for handling our manuscript and the two anonymous reviewers for their constructive comments on our manuscript.

References

Alam, M.A., Parada, M.A., 2013. A note on "Origin of components in Chilean thermal waters" by. J. S. Am. Earth Sci. 2011–2013 http://dx.doi.org/10.1016/j.jsames.2013.09.013.

Aravena, D., Muñoz, M., Morata, D., Lahsen, A., Parada, M.Á., Dobson, P., 2016. Assessment of high enthalpy geothermal resources and promising areas of Chile. Geothermics 59, 1–13. http://dx.doi.org/10.1016/j.geothermics.2015.09.001.

Barton, C.A., Zoback, M.D., Moos, D., 1995. Fluid flow along potentially active faults in crystalline rock. Geology 23, 683. http://dx.doi.org/10.1130/0091-7613(1995)023<0683:FFAPAF>2.3.CO;2.

Barton, C.A., Hickman, S., Morin, R., Zoback, M.D., Benoit, D., 1998. Reservoir-scale fracture permeability in the Dixie V alley, Nevada. Geothermal Field, Proceedings 23rd Workshop on Geothermal Reservoir Engineering, Stanford University, 299–306. Alam, M.A., Parada, M.A., 2013. A note on "Origin of components in Chilean thermal waters" by. J. S. Am. Earth Sci. 2011–2013. http://dx.doi.org/10.1016/j.jsames.2013.09.013.

Bodnar, R.J., 1993. Revised equation and table for determining the freezing point depression of H2O-NaCl solutions. Geochim. Cosmochim. Acta 57, 683–684. http://dx.doi.org/10.1016/0016-7037(93)90378-A.

Browne, P.R.L., 1978. Hydrothermal alteration in active geothermal fields. Annu. Rev. Earth Planet. Sci. 6, 229–248. http://dx.doi.org/10.1146/annurev.ea.06.050178.001305.

Cembrano, J., 1996. The Liquiñe Ofqui fault zone: a long-lived intra-arc fault system in southern Chile. Tectonophysics 259, 55–66. http://dx.doi.org/10.1016/0040-1951(95)00066-6.

Cembrano, J., Lara, L., 2009. The link between volcanism and tectonics in the southern volcanic zone of the Chilean Andes: a review. Tectonophysics 471, 96–113. http://dx.doi.org/10.1016/j.tecto.2009.02.038.

Cox, S.F., 2010. The application of failure mode diagrams for exploring the roles of fluid pressure and stress states in controlling styles of fracture-controlled permeability enhancement in faults and shear zones. Geofluids 217–233 http://dx.doi.org/10.1111/j.1468-8123.2010.00281.x.

Davatzes, N.C., Hickman, S.H., 2010. The Feedback Between Stress, Faulting, and Fluid Flow: Lessons from the Coso Geothermal Field, CA, USA, in: Proceedings World Geothermal Congress 2010 Bali, Indonesia, 25–29 April 2010.

Deditius, a.P., Utsunomiya, S., Ewing, R.C., Chryssoulis, S.L., Venter, D., Kesler, S.E., 2009. Decoupled geochemical behavior of As and Cu in hydrothermal systems. Geology 37, 707–710. http://dx.doi.org/10.1130/G25781A.1.

Dobson, P.F., Kneafsey, T.J., Hulen, J., Simmons, A., 2003. Porosity, permeability, and fluid flow in the Yellowstone geothermal system, Wyoming. J. Volcanol. Geotherm. Res. 123, 313–324. http://dx.doi.org/10.1016/S0377-0273(03)00039-8.

Dobson, P.F., Kennedy, B.M., Reich, M., Sanchez, P., Morata, D., 2013. Effects of volcanism, crustal thickness, and large scale faulting on the He isotope signatures of geothermal systems in Chile. 38th Workshop on Geothermal Reservoir Engineering (p. SGP–TR–198).

Giggenbach, W.F., Goguel, R.L., 1989. Collection and analysis of geothermal and volcanic water and gas discharges. DSIR Report CD-2401, fourth ed..

Günther, D., Audétat, A., Frischknecht, R., Heinrich, C.A., 1998. Quantitative analysis of major, minor and trace elements in fluid inclusions using laser ablation-inductively coupled plasmamass spectrometry. J. Anal. At. Spectrom. 13, 263–270. http://dx.doi.org/10.1039/a707372k.

Hanano, M., 2004. Contribution of fractures to formation and production of geothermal resources. Renew. Sust. Energ. Rev. 8, 223–236. http://dx.doi.org/10.1016/j.rser.2003.10.007.

Hayba, D.O., Ingebritsen, S.E., 1994. The computer model HYDROTHERM, a three-dimensional finite-difference model to simulate ground-water flow and heat

transport in the temperature range of 0 to 1200 °C. U.S. Geol Survey Water-Res Invest Report. 94, p. 12252.
Hayba, D.O., Ingebritsen, S.E., 1997. Multiphase groundwater flow near cooling plutons. J. Geophys. Res. 102, 12235. http://dx.doi.org/10.1029/97JB00552.
Heap, M.J., Kennedy, B.M., Pernin, N., Jacquemard, L., Baud, P., Farquharson, J.I., Scheu, B., Lavallée, Y., Gilg, H.A., Letham-Brake, M., Mayer, K., Jolly, A.D., Reuschlé, T., Dingwell, D.B., 2015. Mechanical behaviour and failure modes in the Whakaari (White Island volcano) hydrothermal system, New Zealand. J. Volcanol. Geotherm. Res. 295, 26–42. http://dx.doi.org/10.1016/j.jvolgeores.2015.02.012.
Hickman, S.H., Barton, C.A., Zoback, M.D., Morin, R., Sass, J., Benoit, R., 1997. In situ stress and fracture permeability along the Stillwater fault zone, Dixie Valley, Nevada. Int. J. Rock Mech. Min. Sci. 34, 414.
Ingebritsen, S.E., Manning, C.E., 1999. Geological implications of a permeability-depth curve for the continental crust. Geology 27, 1107–1110. http://dx.doi.org/10.1130/0091-7613(1999)027<1107:GIOAPD>2.3.CO.
Ingebritsen, S.E., Manning, C.E., 2011. Permeability of the continental crust: dynamic variations inferred from seismicity and metamorphism. Front. Geofluids 193–205. http://dx.doi.org/10.1002/9781444394900.ch13.
Ingebritsen, S.E., Geiger, S., Hurwitz, S., Driesner, T., 2010. Numerical simulation of magmatic hydrothermal systems. Rev. Geophys. 48, RG1002. http://dx.doi.org/10.1029/2009RG000287.
Kim, Y., 2004. Fault damage zones. J. Struct. Geol. 26, 503–517. http://dx.doi.org/10.1016/j.jsg.2003.08.002.
Kostova, B., Pettke, T., Driesner, T., Petrov, P., Heinrich, C.A., 2004. LA ICP-MS Study of Fluid Inclusions in Quartz From the Yuzhna Petrovitsa Deposit, Madan Ore Field, Bulgaria. pp. 25–36.
Lahsen, A., Muñoz, N., Parada, M.A., 2010. Geothermal Development in Chile. World Geotherm. Congr. 2010 pp. 25–29.
Lahsen, A., Rojas, J., Morata, D., Aravena, D., 2015. Exploration for High-Temperature Geothermal Resources in the Andean Countries of South America. World Geotherm. Congr. 2015 pp. 19–25.
Lavenu, A., Cembrano, J., 1999. Compressional- and transpressional-stress pattern for Pliocene and Quaternary brittle deformation in fore arc and intra-arc zones (Andes of Central and Southern Chile). J. Struct. Geol. 21, 1669–1691. http://dx.doi.org/10.1016/S0191-8141(99)00111-X.
Lohmar, S., Stimac, J., Colvin, A., González, A., Iriarte, S., Melosh, G., Wilmarth, M., 2012. Tolhuaca volcano (Southern Chile, 38.3°S): new learnings from surface mapping and geothermal exploration wells. Proceedings Congreso Geológico Chileno 2012 Antofagasta, Chile, 5–9 August 2012, pp. 443–445.
Meller, C., Kohl, T., 2014. The significance of hydrothermal alteration zones for the mechanical behavior of a geothermal reservoir. Geotherm. Energy 2, 12. http://dx.doi.org/10.1186/s40517-014-0012-2.
Melosh, G., Cumming, W., Benoit, D., Wilmarth, M., Colvin, A., Winick, J., Soto-, E., Sussman, D., Urzúa-Monsalve, L., Powell, T., Peretz, A., 2010. Exploration results and resource conceptual model of the Tolhuaca Geothermal Field, Chile. Proceedings World Geothermal Congress 2010 Bali, Indonesia, 25–29 April 2010.
Melosh, G., Moore, J., Stacey, R., 2012. Natural reservoir evolution in the Tolhuaca geothermal field, southern Chile. 37th Workshop on Geothermal Reservoir Engineering Stanford University, Stanford, California, January 31–February 1, 2012. SGP-TR-194.
Moncada, D., Mutchler, S., Nieto, a., Reynolds, T.J., Rimstidt, J.D., Bodnar, R.J., 2012. Mineral textures and fluid inclusion petrography of the epithermal Ag–Au deposits at Guanajuato, Mexico: application to exploration. J. Geochem. Explor. 114, 20–35. http://dx.doi.org/10.1016/j.gexplo.2011.12.001.
Moore, J.N., Simmons, S.F., 2013. More power from below. Science 340 (80), 933–934. http://dx.doi.org/10.1126/science.1235640.
Moore, J.N., Allis, R.G., Nemcok, M., Powell, T.S., Bruton, C.J., Wannamaker, P.E., Raharjo, I.B., Norman, D.I., 2008. The evolution of volcano-hosted geothermal systems based on deep wells from Karaha-Telaga Bodas, Indonesia. Am. J. Sci. 308, 1–48. http://dx.doi.org/10.2475/10.2008.01.
Nemcok, M., Moore, J.N., Allis, R., McCulloch, J., 2004. Fracture development within a stratovolcano: the Karaha-Telaga Bodas geothermal field, Java volcanic arc. Geol. Soc. Lond., Spec. Publ. 231, 223–242. http://dx.doi.org/10.1144/GSL.SP.2004.231.01.13.
Nemčok, M., Moore, J.N., Christensen, C., Allis, R., Powell, T., Murray, B., Nash, G., 2007. Controls on the Karaha–Telaga Bodas geothermal reservoir, Indonesia. Geothermics 36, 9–46. http://dx.doi.org/10.1016/j.geothermics.2006.09.005.
Neuzil, C.E., 1994. How permeable are clays and shales? Water Resour. Res. 30, 145–150. http://dx.doi.org/10.1029/93WR02930.
Niemeyer, H., Muñoz, J., 1983. Hoja de La Laja, Región del Biobío. Servicio Nacional de Geología y Minería, Carta Geológica de Chile 57 (52 p., escala 1:250.000).
Perez, P., Sanchez, P., Arancibia, G., Cembrano, J., Veloso, E., Lohmar, S., Stimac, J., 2012. Sampling and detailed structural mapping of veins, fault-ve nd faults from Tolhuaca Geothermal System, Southern Chile, in: Actas XIII Congreso Geológico Chileno Universidad Católica Del Norte, Antofagasta, Chile. 1 pp. 403–406.
Perez-Flores, P., Veloso, E.E., Cembrano, J.M., Sánchez, P., Iriarte, S., Lohmar, S., 2013. Paleomagnetic Reorientation of Structural Elements in Drill Cores: An Example From Tolhuaca Geothermal Field (Abstract), in: AGU Fall Meeting Abstracts.
Perez-Flores, P., Cembrano, J., Sanchez-Alfaro, P., Veloso, E., Arancibia, G., Roquer, T., 2016. Tectonics, magmatism and paleo-fluid distribution in a strike-slip setting: Insights from the northern termination of the Liquiñe-Ofqui Fault System, Chile. Tectonophysics http://dx.doi.org/10.1016/j.tecto.2016.05.016.
Peterson, E.C., Mavrogenes, J.A., 2014. Linking high-grade gold mineralization to earthquake-induced fault-valve processes in the Porgera gold deposit, Papua New Guinea. Geology 42, 383–386. http://dx.doi.org/10.1130/G35286.1.
Pokrovski, G.S., Borisova, a.Y., Bychkov, a.Y., 2013. Speciation and transport of metals and metalloids in geological vapors. Rev. Mineral. Geochem. 76, 165–218. http://dx.doi.org/10.2138/rmg.2013.76.6.
Reich, M., Deditius, A., Chryssoulis, S., Li, J.-W., Ma, C.-Q., Parada, M.A., Barra, F., Mittermayr, F., 2013. Pyrite as a record of hydrothermal fluid evolution in a porphyry copper system: A SIMS/EMPA trace element study. Geochim. Cosmochim. Acta 104, 42–62. http://dx.doi.org/10.1016/j.gca.2012.11.006.
Roedder, E., Bodnar, R.J., 1997. Fluid inclusion studies of hydrothermal ore deposits. In: Barnes, H.L. (Ed.), Geochemistry of Hydrothermal Ore Deposits. Wiley & Sons, Inc., New York, NY, pp. 657–698.
Rosenau, M., Melnick, D., Echtler, H., 2006. Kinematic constraints on intra-arc shear and strain partitioning in the southern Andes between 38°S and 42°S latitude. Tectonics 25, 1–16. http://dx.doi.org/10.1029/2005TC001943.
Rowland, J.V., Sibson, R.H., 2004. Structural controls on hydrothermal flow in a segmented rift system, Taupo Volcanic Zone, New Zealand. Geofluids 4, 259–283. http://dx.doi.org/10.1111/j.1468-8123.2004.00091.x.
Rowland, J.V., Simmons, S.F., 2012. Hydrologic, magmatic, and tectonic controls on hydrothermal flow, Taupo Volcanic Zone, New Zealand: implications for the formation of epithermal vein deposits. Econ. Geol. 107, 427–457. http://dx.doi.org/10.2113/econgeo.107.3.427.
Sanchez, P., Perez, P., Reich, M., Arancibia, G., Cembrano, J., Campos, E., Lohmar, S., 2013. The influence of fault-fracture network activity on fluid geochemistry and mineral precipitation at the Tolhuaca geothermal system, Southern Chile. Mineral. Mag. 77, 2108–2296. http://dx.doi.org/10.1180/minmag.2013.077.5.19.
Sánchez, P., Pérez-Flores, P., Arancibia, G., Cembrano, J., Reich, M., 2013. Crustal deformation effects on the chemical evolution of geothermal systems: the intra-arc Liquiñe–Ofqui fault system, Southern Andes. Int. Geol. Rev. 55, 1384–1400. http://dx.doi.org/10.1080/00206814.2013.775731.
Sanchez-Alfaro, P., Sielfeld, G., Campen, B.V., Dobson, P., Fuentes, V., Reed, A., Palma-Behnke, R., Morata, D., 2015. Geothermal barriers, policies and economics in Chile—lessons for the Andes. Renew. Sust. Energ. Rev. 51, 1390–1401. http://dx.doi.org/10.1016/j.rser.2015.07.001.
Scott, S., Driesner, T., Weis, P., 2015. Geologic controls on supercritical geothermal resources above magmatic intrusions. Nat. Commun. 6, 7837. http://dx.doi.org/10.1038/ncomms8837.
Secor, D.T., 1965. Role of fluid pressure in jointing. Am. J. Sci. 263, 633–646. http://dx.doi.org/10.2475/ajs.263.8.633.
Simmons, S.F., Browne, P., 2000. Hydrothermal minerals and precious metals in the Broadlands-Ohaaki geothermal system: implications for understanding low-sulfidation epithermal environments. Econ. Geol. 95, 971–999. http://dx.doi.org/10.2113/95.5.971.
Simmons, S.F., White, N., John, D., 2005. Geological characteristics of epithermal precious and base metal deposits. Econ. Geol. 485–522 (100th Anni).
Tembe, S., Lockner, D.a., Wong, T.F., 2010. Effect of clay content and mineralogy on frictional sliding behavior of simulated gouges: Binary and ternary mixtures of quartz, illite, and montmorillonite. J. Geophys. Res. Solid Earth 115, 1–22. http://dx.doi.org/10.1029/2009JB006383.
Thiele, R., Lahsen, A., Hugo, M., Varela, J., Munizaga, F., 1987. Estudio geológico regional a escala 1:100.000 de la Hoya Superior y Curso Medio del Río Bío-Bío. Centrales Quitramán, Huequecura, Aguas Blancas, Pangue, Ralco y Llanquén. Depto. de Geología-ENDESA (In spanish).
Weis, P., Driesner, T., Heinrich, C.A., 2012. Porphyry-copper ore shells form at stable pressure-temperature fronts within dynamic fluid plumes. Science 338, 1613–1616. http://dx.doi.org/10.1126/science.1225009.
Wiprut, D., Zoback, M.D., 2000. Fault reactivation and fluid flow along a previously dormant normal fault in the northern North Sea. Geology 28, 595. http://dx.doi.org/10.1130/0091-7613(2000)28<595:FRAFFA>2.0.CO;2.
Wyering, L.D., Villeneuve, M.C., Wallis, I.C., Siratovich, P.a., Kennedy, B.M., Gravley, D.M., Cant, J.L., 2014. Mechanical and physical properties of hydrothermally altered rocks, Taupo Volcanic Zone, New Zealand. J. Volcanol. Geotherm. Res. 288, 76–93. http://dx.doi.org/10.1016/j.jvolgeores.2014.10.008.
Zang, A., Stephansson, O., Heidbach, O., Janouschkowetz, S., 2012. World stress map database as a resource for rock mechanics and rock engineering. Geotech. Geol. Eng. 30, 625–646. http://dx.doi.org/10.1007/s10706-012-9505-6.